Clinopyroxene-liquid thermometers and barometers specific to alkaline differentiated magmas

Masotta M.[1,2], *Mollo S.*[3], *Freda C.*[3], *Gaeta M.*[2,3], *Moore G.*[4]

[1] Bayerisches Geoinstitut, Universität Bayreuth, Bayreuth, Germany

[2] Dipartimento di Scienze della Terra, Sapienza Università di Roma, Italy

[3] Istituto Nazionale di Geofisica e Vulcanologia, Roma, Italy

[4] Department of Earth and Environmental Sciences, University of Michigan, MI (USA)

Corresponding author:

Matteo Masotta

Bayerisches Geoinstitut, Universität Bayreuth, Bayreuth, Germany

E-mail: matteo.masotta@uni-bayreuth.de

Abstract

We present new thermometers and barometers based on clinopyroxene-liquid equilibria specific to alkaline differentiated magmas. The new models were calibrated through regression analyses of experimental datasets obtained by merging phase equilibria experiments from literature with new experiments performed by using trachytic and phonolitic starting compositions. The regression strategy was twofold: i) we have tested previous thermometric and barometric equations and recalibrated these models using the new datasets; ii) we have calibrated a new thermometer and a new barometer including only regression parameters that closely describe the compositional variability of the datasets. The new models yield more precise estimates than previous thermometers and barometers when used to predict temperatures and pressures of alkaline differentiated magmas. We have tested the reliability of the new equations by using clinopyroxene-liquid pairs from trachytes and phonolites erupted during major explosive eruptions at the Phlegrean Fields and Mt. Vesuvius (central Italy). The test yielded crystallization conditions comparable to those determined by means of melt and fluid inclusion analyses and phase equilibria studies; this validates the use of the proposed models for precise estimates of crystallization temperatures and pressures in differentiated alkaline magmas. Because these magmas feed some of the most voluminous, explosive, and threatening volcanic eruptions in the world, a better understanding of the environmental conditions of their reservoirs is mandatory and this is now possible with the new models provided here.

1. Introduction

Clinopyroxene is widespread in igneous rocks and its composition is routinely used to shed light on the processes of magma generation and crystallization conditions. For this reason, a large number of thermometers and barometers that use either clinopyroxene composition alone or clinopyroxene-liquid equilibria are available (Nimis 1995; Nimis and Ulmer 1998; Nimis and Taylor 2000; Putirka et al. 1996, 2003; Putirka 2008). These models are derived from regression analyses of experimental data obtained under variable conditions of pressure, temperature and melt composition; consequently, their precision mostly depends on i) the quality and number of experimental data incorporated into or excluded from the calibration dataset (Putirka 2008), and ii) the compositional bounds of the calibration dataset relative to the natural compositions used as input data. Nevertheless, even thermometers and barometers calibrated using a large number of experiments may yield imprecise temperature and pressure estimates of magma compositions that are not adequately represented in the calibration dataset. The experimental data in published

literature used to calibrate thermometers and barometers mostly consist of phase equilibria experiments performed with compositions ranging from basalt to rhyolite, whereas experiments performed with alkaline differentiated compositions (i.e., phonolite and trachyte) are scarcely represented in these datasets.

Alkaline differentiated melts are frequently associated with explosive volcanic eruptions (e.g., Pabst et al. 2008; Fontijn et al. 2010; White et al. 2012) and with caldera-forming events emplacing large volumes of magma (~10 km^3, e.g., Marianelli et al. 2006; Masotta et al. 2010). Using a combination of geochemical/petrological/geophysical models, a better understanding of the reservoirs that feed explosive eruptions is now possible. In this regard, clinopyroxene and melt compositions are readily available and easily analyzable in volcanic rocks, providing valuable constraints on the state of the magma reservoir at the time of the eruption.

In this study, we have developed new thermometric and barometric models calibrated for alkaline differentiated magmas (i.e., clinopyroxene-bearing phonolite and trachyte rocks). The calibration datasets consist of phase equilibria experiments reported in published literature, and newly performed phase equilibria experiments on phonolitic and trachytic magma compositions. Thermometric and barometric equations from Putirka et al. (1996) and Putirka (2008) were tested and recalibrated using the new alkaline datasets, yielding to a significant improvement of their prediction. Eventually, the regression parameters of the best predictive equations were modified in order to capture the variability of the alkaline datasets and a new thermometer and barometer were obtained by new regression analysis.

Tests performed on a sample population of the dataset demonstrate the reliability of the new thermometric and barometric models in predicting clinopyroxene crystallization temperatures and pressures in alkaline differentiated magmas. Therefore, in order to provide an immediate application of the new models, we have used clinopyroxene-liquid pairs from the Phlegrean Fields and Mt. Vesuvius as input data for the new thermometer and barometer. The new thermometer and barometer provide reliable estimates of temperatures and pressures, in accordance with those determined from fluid and melt inclusion data, in addition to phase equilibria studies.

2. Methods

2.1 Starting materials

As starting materials for phase equilibria experiments we have used two volcanic rocks belonging to different Italian magmatic systems. The first rock is a pumice from the Tufo Giallo della Via Tiberina explosive eruption (Sabatini Volcanic District, central Italy). This product is K-phonolitic in composition and is one of the most differentiated, silica-saturated alkaline products in

central Italy (Masotta et al. 2010; 2012a). The second rock is a lava flow from the Grotta dei Palizzi (Vulcano island, Aeolian Arc, southern Italy). This sample is trachytic in composition, and is representative of alkaline differentiated magmas feeding the recent activity of La Fossa Volcano (De Astis et al. 1997). With respect to the starting materials used in previous experimental studies (Fabbrizio and Carroll 2008; Andujar et al. 2008, 2010), our phonolite and trachyte are slightly less differentiated, showing K_2O/Na_2O ratios of 0.3 and 2.6, respectively (see Table 1).

2.2 Experimental and analytical methods

Approximately 20 g of each of the two starting materials were reduced to powder in an agate mortar. Each powdered sample was loaded in a Fe pre-saturated Pt-crucible and melted twice in a 1-atm furnace at 1400 °C for 1 h. Resulting glasses were analysed by scanning electron microscope to check for homogeneity and presence of crystalline phases. Experiments were conducted in a ¾" non-end loaded piston cylinder ("QUICKpress" design by Depths of the Earth Co.) at the Department of Chemistry and Biochemistry (Arizona State University, USA). All the runs were performed at 2 kbar by means of 25 mm assemblies specifically designed for low-pressure experiments (see Masotta et al. 2012b for further details). The fO_2 imposed by the assembly of the piston cylinder is NNO+2 (Masotta et al., 2012a; 2012b). This value matches with the redox state frequently estimated for phonolitic and trachytic magmas via geochemical modelling (e.g., White et al., 2012) or by comparing natural and experimental phase proportions and compositions (Andujar et al. 2008; Freda et al. 2008). The assembly was cold pressurized to a nominal pressure 10% higher than that desired for the experiment and kept constant for few minutes. Pressure was then decreased to 2 kbar and maintained constant for the duration of the experiment and during quench. Phase equilibria experiments were performed within the temperature range 850-950 °C and 900-1000 °C for the phonolite and trachyte, respectively (Table 2). The temperature was measured using factory calibrated K-type (chromel-alumel) thermocouples with an uncertainty of ±5 °C. Due to the role played by both H_2O and CO_2 in alkaline magmas (e.g., Esposti Ongaro et al. 2006), the experiments were performed using different proportions of the two volatile species. Both species were added directly into the charge as follows: from 1.5 to 5.36 wt.% of H_2O was added with a microsyringe, whereas from 0.11 to 0.4 wt.% of CO_2 was added in the form of Ag_2CO_3 powder mixed with the starting material (Table 2).

Field Emission-Scanning Electron Microscope (FE-SEM) images and electron microprobe analyses (EMPA) of experimental products were obtained at the HP-HT Laboratory of Experimental Volcanology and Geophysics (Istituto Nazionale di Geofisica e Vulcanologia, Rome, Italy) with a JEOL FE-SEM 6500F equipped with an energy dispersive microanalysis system and a

JEOL-JXA8200 EDS-WDS combined electron microprobe, respectively. The electron microprobe is equipped with five wavelength-dispersive spectrometers. Glasses were analyzed using 15 kV accelerating voltage and 10 nA beam current, with a defocused electron beam of 5 μm and a counting time of 5 s on background and 15 s on peak, whereas for crystals, a beam size of 2 μm and counting time of 20 and 10 s on peaks and background were used, respectively. The following standards have been adopted for the various chemical elements: jadeite (Si and Na), labradorite (Al and Ca), forsterite (Mg), andradite (Fe), rutile (Ti), orthoclase (K), barite (Ba), apatite (P) and spessartine (Mn). Sodium and potassium were analysed before other elements to reduce possible volatilization effects.

2.3 Liquid and clinopyroxene components

In this study liquid components have been calculated as cation fractions following Putirka (1999). Conversely, clinopyroxene components have been determined using the procedures reported in Putirka et al. (1996) and then slightly modified in Putirka (1999). Molecular components were calculated on the basis of six oxygen atoms and the charge balance equation of Lindsley (1983) was applied to all the analyses for determining Fe^{3+}. The jadeite (Jd, $NaAlSi_2O_6$) component is the amount of Na or octahedral Al ($Al^{VI} = Al^{tot} - Al^{IV}$; $Al^{IV} = 2\text{-}Si$), whichever is less. When the CrCa-Tschermak component (CrCaTs, $CaCr_2SiO_6 = Cr/2$) is calculated, then the Ca-Tschermak (CaTs, $CaAl^{VI}Al^{IV}SiO_6$) component results equal to any remaining Al^{VI} ($CaTs = Al^{VI}$ - Jd). The Al^{IV} in excess is used to form CaTi-Tschermak (CaTiTs, $CaTiAl_2O_6 = (Al^{IV} – CaTs)/2$) and CaFe-Tschermak (CaFeTs, $CaFeSiAlO_6$) components. All calcium remaining after forming Ts, i.e. the sum of CaTs, CaFeTs, CrCaTs and CaTiTs, gives diopside (Di, $CaMgSi_2O_6$) and hedenbergite (Hd, $CaFeSi_2O_6$) components, i.e., DiHd = Ca – Ts. Only Mg and Fe^{2+} are used for calculation of the enstatite (En, $Mg_2Si_2O_6$) and ferrosilite (Fs, $Fe_2Si_2O_6$). The enstatite-ferrosilite (EnFs) component is equal to one-half the FeO+MgO (Fm) component remaining after forming DiHd (EnFs = (Fm - DiHd)/2). At the equilibrium condition, clinopyroxene components calculated following this scheme should be very close to unity (see also Putirka et al. 1996; Putirka 1999).

2.4 Dataset and regression strategy

The dataset used to calibrate the thermometers consists of 81 clinopyroxene-liquid pairs obtained by merging our new phase equilibria experiments with previously published experiments on trachyte and phonolite magmas from (i) Laacher See Volcano (Germany; Berndt et al. 2001), (ii) Phlegrean Fields (Italy; Fabbrizio and Carrol 2008), (iii) Tenerife Island (Canary Island, Spain; Andujar et al. 2008, 2010; Andujar and Scaillet 2012), and (iv) Sabatini Volcanic District (Italy,

Masotta et al. 2012a). Overall, the experimental dataset includes experiments with trachytic and phonolitic melt compositions (i.e., SiO_2 = 53-69 wt.% and Na_2O+K_2O = 10-17 wt.%; Figure 1), equilibrated at 700-1000 °C and 0.5-3 kbar (the whole dataset is reported in Table 1EA). In order to increase the leverage on pressure estimates of the barometric equations, we have extended the calibration dataset by adding 61 clinopyroxene-liquid pairs equilibrated at high-pressures (up to 15 kbar; the additional dataset is reported in Table 2EA). A detailed discussion on this strategy is reported below.

Two different regression strategies have been adopted to derive new and more precise thermometers and barometers: 1) the alkaline dataset was used to recalibrate models T1, T2, T3, T4, P1 and P2 of Putirka et al. (1996), and models Eqn. 33 and Eqn. 32c of Putirka (2008); 2) new regression models were developed including only those parameters that closely describe the variance of the dataset (cf. Putirka et al. 1999), whereas all parameters producing data overfitting were removed from the regression analysis (Jefferys and Berger 1992; Ratkowsky 1990). It is worth noting that we have based our new thermometric and barometric models on previous equations by Putirka et al. (1996) and Putirka (2008), because of their frequent application to volcanologic studies and their calibration at temperature and pressure conditions that include those typical of alkaline differentiated magmas (e.g., Mollo et al., 2010a; 2010b). In contrast, other available thermometers and barometers have been calibrated at pressures and temperatures contrasting with those of interest for this study (e.g., 1077-2177 °C and 10-30 kbar; Putirka, 1999; Putirka et al., 2003).

The equations recalibrated with the new experimental dataset are:

$$T1 \qquad \frac{10^4}{T(K)} = a + b\ln\left(\frac{X_{Jd}^{cpx} X_{Ca}^{liq} X_{Fm}^{liq}}{X_{DiHd}^{cpx} X_{Na}^{liq} X_{Al}^{liq}}\right) + c\ln\left(\frac{X_{Mg}^{liq}}{X_{Mg}^{liq} + X_{Fe}^{liq}}\right) + d\ln\left(X_{Ca}^{liq}\right)$$

$$T2 \qquad \frac{10^4}{T(K)} = a + b\ln\left(\frac{X_{Jd}^{cpx} X_{Ca}^{liq} X_{Fm}^{liq}}{X_{DiHd}^{cpx} X_{Na}^{liq} X_{Al}^{liq}}\right) + c\ln\left(\frac{X_{Mg}^{liq}}{X_{Mg}^{liq} + X_{Fe}^{liq}}\right) + d\ln\left(X_{Ca}^{liq}\right) + eP(kbar)$$

$$T3 \qquad \frac{10^4}{T(K)} = a + b\ln\left(\frac{X_{CaTs}^{cpx} X_{Si}^{liq} X_{Fm}^{liq}}{X_{DiHd}^{cpx} X_{Al}^{liq}}\right) + c\ln\left(\frac{X_{Mg}^{liq}}{X_{Mg}^{liq} + X_{Fe}^{liq}}\right) + d\ln\left(\frac{1}{(X_{Al}^{liq})^2}\right)$$

$$T4 \qquad \frac{10^4}{T(K)} = a + b\ln\left(\frac{X_{CaTs}^{cpx} X_{Sia}^{liq} X_{Fm}^{liq}}{X_{DiHd}^{cpx} X_{Al}^{liq}}\right) + c\ln\left(\frac{X_{Mg}^{liq}}{X_{Mg}^{liq} + X_{Fe}^{liq}}\right) + d\ln\left(\frac{1}{(X_{Al}^{liq})^2}\right) + eP(kbar)$$

$$Eq.\ 33 \qquad \frac{10^4}{T(K)} = a + b\ln\left(\frac{X_{Jd}^{cpx} X_{CaO}^{liq} X_{Fm}^{liq}}{X_{DiHd}^{cpx} X_{Na}^{liq} X_{Al}^{liq}}\right) + c\left(H_2O^{liq}\right) + d\left(X_{CaO}^{liq} X_{SiO_2}^{liq}\right) +$$
$$+ e\ln\left(X_{TiO_2}^{liq}\right) + f\left(X_{NaO_{0.5}}^{liq} + X_{KO_{0.5}}^{liq}\right) + g\left(Mg\#^{liq}\right) + h\ln\left(X_{EnFs}^{cpx}\right) + iP(kbar)$$

$$P1 \qquad P(kbar) = a + b\frac{T(K)}{10^4} + c\frac{T(K)}{10^4}\ln\left[\frac{X_{Jd}^{cpx}}{X_{Na}^{liq}X_{Al}^{liq}\left(X_{Si}^{liq}\right)^2}\right] + d\left(X_{Na}^{liq} + X_{Al}^{liq}\right)$$

$$P2 \qquad P(kbar) = a + b\frac{T(K)}{10^4} + c\frac{T(K)}{10^4}\ln\left[\frac{X_{Jd}^{cpx}}{X_{Na}^{liq}X_{Al}^{liq}\left(X_{Si}^{liq}\right)^2}\right] + d\frac{T(K)}{10^4}\ln\left[\frac{1}{X_{Na}^{liq} + X_{Al}^{liq}}\right]$$

$$Eq.\,32c \qquad P(kbar) = a + bT(K) + c\left(X_{FeO}^{liq}\right) + d\left(X_{CaTs}^{cpx}\right) + e\left(H_2O^{liq}\right) + f\left(X_{CaO}^{liq}X_{SiO2}^{liq}\right) + g\left(\frac{X_{Al}^{cpx}}{X_{AlO1.5}^{liq}}\right)$$

The value of each regression parameter is reported in Table 3 together with the standard error of estimate (SEE) of the regression analysis. Thermometric equations T1 and T2 are formulated for clinopyroxene-liquid equilibria based on DiHd-Jd exchange reaction, whereas equations T3 and T4 are based on DiHd-CaTs equilibrium (Putirka et al. 1996); notably, the exchange equilibrium of equations T2 and T4 is also slightly sensitive to pressure. Equation 33 is a DiHd-Jd thermometer obtained by global calibrations of experiments conducted at P< 70 kbar (Putirka 2008). Conversely, barometric equations P1 and P2 are calibrated using the pressure-dependency of Jd on the large partial molar volumes for Na and Al oxides in basaltic liquids, combined with the small partial molar volume of jadeite in clinopyroxene (Putirka et al. 1996). Equation 32c is a barometer based on the partitioning of Al between clinopyroxene and liquid, which also considers the effects of water and temperature (Putirka 2008).

3. Results and Discussion

3.1 Phase equilibria experiments

The mineral assemblage of our experimental charges invariably consists of clinopyroxene, plagioclase and sanidine (Table 2). In the experiments performed with phonolite, clinopyroxene and plagioclase are ubiquitous in all sub-*liquidus* runs and sanidine occurs at T< 925 °C. In the experiments performed with trachyte, clinopyroxene is always present, whereas plagioclase and sanidine appear at T< 950 °C and T< 900 °C, respectively. Crystals are euhedral showing either prismatic (clinopyroxene) or tabular (sanidine and plagioclase) shapes, with sizes ranging from 6 to 10 μm in experiment with phonolite and from 8 to 12 μm in experiments with trachyte (Figure 2). We can attest that clinopyroxenes and coexisting melts approached equilibrium as testified by: (i) the experimental duration comparable to that necessary to obtain a homogeneous phase assemblage in alkaline magmas (Mollo et al. 2013a) and (ii) the simultaneous occurrence of euhedral, unzoned crystals and compositionally homogeneous melts. It is also worth noting that, by means of different

thermal pre-treatments and reversal experiments, Mollo et al. (2013a) have observed that alkaline magma compositions do not show significant delay of crystal nucleation or change in phase assemblage and proportion.

The mg-*number* [*mg*-number = MgO/(MgO+FeO_{tot})] of both clinopyroxenes and coexisting melts progressively increases with increasing temperature and H_2O content (Tables 4 and 5), showing good correspondence with other experimental data obtained for alkaline compositions (Del Gaudio et al. 2010; Mollo et al. 2010b). As a test for equilibrium we have used the T-sensitive model for Fe-Mg exchange [$K_D(Fe\text{-}Mg)^{cpx\text{-}liq}$ = molar ratio of $(Fe/Mg)^{cpx}/(Fe/Mg)^{liq}$] of Putirka (2008):

$$\ln K_D(Fe-Mg)^{cpx-liq} = -0.107 - \frac{1719}{T(K)}$$

(Equation 35; $R^2 = 0.12$; SEE = 0.08)

This model is calibrated by assuming Fe^{2+} as total iron and is based on the deviations between observed and calculated values for $K_D(Fe\text{-}Mg)^{cpx\text{-}liq}$ resulting from experimental clinopyroxene-liquid pairs equilibrated at variable temperatures. Notably, the assumption of Fe^{2+} as total iron in clinopyroxene and coexisting melt is valid providing that: i) phase compositions in natural samples are calculated following the same procedure used for experimental phases in the calibration dataset; ii) the range of experimental fO_2 matches that of natural samples to which the model is applied (as in this study). Moreover, in the range of fO_2 conditions of natural alkaline magmas, this parameter does not change the phase relations (Andujar and Scaillet, 2012) but mimics temperature by affecting the amount and composition of crystals (Mollo et al., 2013b).

The T-sensitive model of Putirka (2008) predicts $K_D(Fe\text{-}Mg)^{cpx\text{-}liq}$ values significantly different to those experimentally determined for the clinopyroxene-liquid pairs of the calibration dataset (0.15-0.23 and 0.09-0.37, respectively; Figure 3). This finding highlights that the alkaline compositions are scarcely represented into the calibration datasets used by Putirka (2008). Therefore, we have recalibrated this model introducing an additional parameter defined as Na-number [Na-*number* = $X_{Na}^{liq} / (X_{Na}^{liq} + X_K^{liq})$], which considers the alkali content of the melt, obtaining the following equation:

$$K_D(Fe\text{-}Mg)^{cpx\text{-}liq} = \exp\left(1.735 - 3.056\frac{10^3}{T(K)} - 1.668\frac{X_{Na}^{liq}}{X_{Na}^{liq} + X_K^{liq}}\right)$$

(Kd_alk; $R^2 = 0.58$; SEE = 0.05)

The introduction of the Na-*number* as new parameter of the regression remarkably improved the precision of the T-sensitive model, despite the new equation is evidently useful for trachyte and phonolite magmas only.

3.2 New regression analyses based on previous activity models

Clinopyroxene-liquid pairs from the alkaline datasets have been used to test the precision of previous thermometers and barometers. For each regression analysis we have calculated the standard error of estimate (SEE), which represents the formal error of a model and is analogous to the standard deviation of a mean (see Putirka et al. 1996). Results from our calculations indicate that both thermometric equations T1 and T2 of Putirka et al. (1996), based on DiHd-Jd exchange reaction, overestimate the crystallization temperature of clinopyroxene (Figure 4) yielding SEE_{T1} = 120 °C and SEE_{T2} = 127 °C. Similarly, equations T3 and T4 yield SEE_{T3} = 145 °C and SEE_{T4} = 154 °C, respectively. It is worth noting that CaTs is less abundant relative to other components and is not ubiquitous in clinopyroxene (Table 1EA submitted online as supplementary material). This means that the number of experimental data used to calibrate and test each activity model based on DiHd-CaTs equilibrium (i.e., equations T3 and T4) is insufficient to obtain precise estimates (Figure 4). Moreover, due to aluminium enrichments during rapid growth of crystals, the equilibrium condition is more difficult to assess for Tschermakitic molecules (Mollo et al. 2010b, 2011, 2012).

With respect to early thermometric models proposed by Putirka et al. (1996), a larger experimental dataset was used for the global calibration of equation 33 of Putirka (2008). This more recent model predicts the clinopyroxene crystallization temperature of alkaline magmas much better than previous models (SEE_{33} = 31.4 °C, Figure 4). The increased number of regression parameters in equation 33 (9 parameters, rather than 4-5 of previous models T1-T4) has significantly improved the precision of this model, although large overestimates persist at temperatures below 850 °C (Figure 4).

Barometric equations P1 and P2 of Putirka et al. (1996) systematically underestimate the clinopyroxene crystallization pressure yielding SEE_{P1} = 7.3 kbar and SEE_{P2} = 9.5 kbar (Figure 5). Conversely, equation 32c of Putirka (2008), being calibrated for a broader range of compositions than equations P1 and P2, yields the more accurate estimates (SEE_{32c} = 2.9 kbar, Figure 5).

We have recalibrated the thermometers and barometers of Putirka et al. (1996) and Putirka (2008) using the same clinopyroxene-liquid pairs used as test data. All these equations were renamed by adding “alk” to the name, i.e., Talk1, Talk2, Talk3, Talk4, Talk33, Palk1, Palk2 and

Palk32c. The original regression parameters by Putirka et al. (1996) and Putirka (2008) and those obtained by our recalibrations are reported in Table 3. Given the restricted compositional bounds of the dataset, recalibrated equations show much lower errors than the original equations. In particular, equations Talk1 and Talk2 (SEE_{Talk1} = 31.6 °C and SEE_{Talk2} = 31.2 °C) produce a slightly better fit to the experimental data than equations Talk3 and Talk4 (SEE_{Talk3} = 33.6 °C and SEE_{Talk4} = 33.9 °C; Figure 5), confirming the scarce correlation of K[DiHd-CaTs] and Al^{liq} with temperature. The increased number and leverage of regression parameters of equation Talk33, yields the best precision among the recalibrated models (SEE_{Talk33} = 24.0 °C).

Notably, the recalibration of the barometric equations did not yield to improved precision, because of the relatively small pressure range of the experimental dataset (0.5-3 kbar). Although the recalibrated models showed relatively low standard error of estimates (SEEs as low as 0.4 kbar), they left unexplained most of the variability internal to the dataset (i.e., coefficients of determination R^2 as low as 0.25). Therefore, any clinopyroxene-liquid pair used as input data yielded pressure estimates between 1 and 2 kbar, independently from the pressure at which it equilibrated. Therefore, in order to increase the leverage on pressure prediction, we included in the calibration dataset additional 61 clinopyroxene-liquid pairs from experiments performed at pressure between 3 and 15 kbar. These compositions were downloaded from the LEPR database (http://lepr.ofm-research.org) and comprise peralkaline rocks used by Putirka (1996) to calibrate early thermometers and barometers (Table 2EA), as well as basaltic to rhyolitic rocks with both alkaline and sub-alkaline affinity. It is worth nothing that, after substantial data screening, this "extended calibration dataset" was selected to significantly improve the precision of barometers by Putirka et al. (1996) and Purirka (2008) for trachyte and phonolite magmas. In this view, our recalibrated equations Palk1, Palk2 and Palk32c show standard errors on estimates two to five times lower than those of previous models (SEE_{Palk1} = 1.71 kbar, SEE_{Palk2} = 1.70 kbar and $SEE_{Palk32c}$ = 1.67 kbar; Figure 5).

3.3 Calibration and test of a new thermometer and barometer

Using our experimental dataset specific to alkaline differentiated magmas, we have calibrated a new clinopyroxene-liquid thermometer and barometer (see the downloadable Excel spreadsheet submitted online as supplementary material) whose equations are:

$$Talk2012 \qquad \frac{10^4}{T(\text{K})} = 2.91 - 0.40\ln\left(\frac{X_{Jd}^{cpx} X_{Ca}^{liq} X_{Fm}^{liq}}{X_{DiHd}^{cpx} X_{Na}^{liq} X_{Al}^{liq}}\right) + 0.038(H_2O) - 1.64\left(\frac{\frac{X_{Mg}^{liq}}{X_{Mg}^{liq} + X_{Fe}^{liq}}}{X_{DiHd}^{cpx}}\right) +$$

$$+1.01\frac{X_{Na}^{liq}}{X_{Na}^{liq} + X_{K}^{liq}} - 0.22\ln\left(X_{Ti}^{liq}\right) + 0.47\ln\left(\frac{X_{Jd}^{cpx}}{X_{Na}^{liq} X_{Al}^{liq} (X_{Si}^{liq})^2}\right) + 1.62\left(K_{D(Fe-Mg)}^{cpx-liq}\right) + 23.39\left(X_{Ca}^{liq} X_{Si}^{liq}\right)$$

(Equation Talk2012; $R^2 = 0.93$; SEE = 18.2)

$$Palk2012 \qquad P(kbar) = -3.89 + 0.28\left[\frac{X_{Jd}^{cpx}}{X_{Na}^{liq} X_{Al}^{liq} \left(X_{Si}^{liq}\right)^2}\right] + 0.074(H_2O) + 5.01\left(\frac{X_{Na}^{liq}}{X_{Na}^{liq} + X_{K}^{liq}}\right) +$$
$$+6.39\left(\text{K}_\text{D}(\text{Fe-Mg})^{\text{cpx-liq}}\right)$$

(Equation Palk2012; $R^2 = 0.80$; SEE = 1.15)

The use of more appropriate parameters, such as the melt Na-*number* and $K_D(Fe\text{-}Mg)^{cpx\text{-}liq}$, has improved the precision of the model Talk2012, whose uncertainty ($SEE_{Talk2012}$ = 18.2 °C) is reduced of about 6-15 °C with respect to the standard error of estimate of recalibrated equations Talk1, Talk2, Talk3, Talk4 and Talk33, and of about 13 °C with respect to SEE_{33} of the best predictive equation 33 of Putirka (2008) (Table 3 and Figure 6). Notably, the model Talk2012 is independent from pressure and the number of sensible parameters is decreased from 14 to 9. Similarly, equation Palk2012 is independent from temperature and comprises a reduced number of parameter compared to equation Palk32 (5 instead of 7). The precision of model Palk2012 ($SEE_{Palk2012}$ = 1.15 kbar) is slightly improved relative to that of the recalibrated equations Palk1, Palk1 and Palk32c, but remarkably improved with respect to that of equation 32c from Putirka (2008) (Table 3 and Figure 6).

In order to verify the accuracy of equations Talk2012 and Palk2012, we have recalibrated these models after subtracting about 25% of clinopyroxene-liquid pairs from the calibration dataset and used these pairs (20 for the thermometer and 35 for the barometer) to test their prediction. Both the recalibrated models predict temperatures and pressures comparable to those predicted by equations Talk2012 and Palk2012 (Figure 7).

3.4 Limits and advantages of the new thermometer and barometer

As demonstrated in this study, the compositional bounds of the calibration dataset are important limiting factors for thermometers and barometers that are based on the regression analysis

of experimental data. Our thermometer, specific to phonolitic and trachytic magmas, is more precise than those from previous studies, but any attempt to use it on compositions different from those of the calibration dataset would produce high errors of estimate. To test the limits of the model Talk2012, we have used as input data clinopyroxenes coexisting with tephri-phonolitic and phono-tephritic liquids (Table 3EA) experimentally obtained at 1000-1300 °C and 0.001-5 kbar (Freda et al. 1997, 2008; Conte et al. 2009; Mollo et al. 2010a, 2010b). Results from these calculations have been compared with those predicted by equations 33 and 32c of Putirka (2008) (Figure 8). Equation Talk2012 generally yields higher errors on temperature estimate than equation 33 of Putirka (2008) ($ETE_{Talk2012}$ = 5-297 °C; ETE_{33} = 3-207 °C; Figure 8). In fact, $SEE_{Talk2012}$ (125 °C) is higher than SEE_{33} (87 °C), confirming the scarce precision of the new thermometer outside its calibration bounds. Conversely, errors on pressure estimate of equation Palk2012 are much lower than those associated to equation 32c of Putirka (2008) ($EPE_{Palk2012}$ = 0.07-45.9 kbar; EPE_{32c} = 0.7-12 kbar; Figure 8). Accordingly, $SEE_{Palk2012}$ (3.4 kbar) is about two times lower than SEE_{32c} (6.5 kbar). However, we must stress out that the better precision of Equation Palk2012 is due to the more restricted pressure range of the calibration dataset (0.5-15 kbar) relative to that (0.001-80 kbar) of Putirka (2008). Therefore, the global equations of Putirka (2008) still represent the best choice to estimate the crystallization conditions of poorly differentiated alkaline magmas and other magma compositions not sufficiently represented in our datasets.

4. Application of the new models to natural case studies

The volcanoes of the Phlegrean Fields and Mt. Vesuvius belong to the potassic alkaline province of Central Italy. These volcanoes are among the most dangerous in the world, threatening the city of Naples and its densely inhabited suburbs. The highly explosive activity at the Phlegrean Fields and Mt. Vesuvius, indeed, represents a continuous menace to more than one million people. With this perspective, it is extremely important to develop new and more precise methods for deciphering crystallization conditions of magmas feeding these eruptions. This will permit to better understand magma chamber processes and to prepare reliable hazard maps (e.g., Cioni et al. 1998; Marianelli et al. 2006; Zollo et al. 2003; Scaillet et al. 2008; Cioni et al. 2003; Todesco et al. 2006). To contribute to these efforts, we have used natural clinopyroxene-liquid compositions from major eruptions at the Phlegrean Fields and Mt. Vesuvius as input data for our new thermometer and barometer (see Table 4EA submitted online as supplementary material). Crystallization temperatures and pressures predicted by our models are in good agreement with those determined via different and independent geochemical models, thus validating their use to reconstruct thermobarometric conditions of these magmatic systems.

Phlegrean Fields

The Phlegrean Fields caldera is located within the Campanian Plain and includes a subaerial and a submerged part, which cover a total area of about 230 km^2. It is a resurgent nested structure formed during two major caldera collapses related to the eruptions of the Campanian Ignimbrite (200 km^3 of trachytic to phono-trachytic pyroclastic-fall and -flow deposits) and the Neapolitan Yellow Tuff (40 km^3 of latitic to trachytic pyroclastic-fall and -flow deposits), respectively (Pabst et al. 2008 and references therein). Volcanic rocks younger than the Neapolitan Yellow Tuff show compositions from shoshonite to peralkaline phonolite with trachyte and alkali-trachyte as the most abundant (Pabst et al. 2008 and references therein). The volcanic system is still active, as demonstrated by fumarolic and seismic activity, and by recurrent repetitive episodes of unrest in the past 30 years (Orsi et al. 1999 and references therein). Melt inclusion data of minerals in rocks younger than 39 ka indicate different depths of crystallization at about 10 km and between 8 and 3 km, suggesting the occurrence of both deep and shallow magma reservoirs (e.g., Marianelli et al. 2006).

On the basis of feldspar-liquid equilibria of trachytic to phono-trachytic pumice samples of the Campanian Ignimbrite, Fedele et al. (2009; and references therein) have suggested crystallization temperatures between 840 and 960 °C. Using a two-feldspar thermometer and melt and fluid inclusions in clinopyroxene and K-feldspar, Fulignati et al. (2004) determined a pre-eruptive temperature of the Breccia Museo magma (a proximal unit belonging to the caldera-forming phase of the Campanian Ignimbrite; Fedele et al. 2009) between 870 and 980 °C. In a more recent study on melt inclusions (Marianelli et al. 2006), the crystallization of clinopyroxene was estimated at temperatures between 870 and 1080 °C. To better constrain the temperature conditions of the Campanian Ignimbrite magma, we have used clinopyroxene-liquid pairs (206 in total) reported in Signorelli et al. (1999), Fulignati et al. (2004) and Fedele et al. (2008) as input data for our new equations Talk2012 and Palk2012 (Table 4EA). In particular, data from Signorelli et al. (1999) refer to the lower and upper fall units of the Campanian Ignimbrite eruption; whereas, those from Fulignati et al. (2004) and Fedele et al. (2009) belong to the Breccia Museo eruption. We have assumed a melt-water content of 3 wt.% according to literature data (Signorelli et al. 1999; Fowler et al. 2007 and references therein). Notably, we have tested that a melt-water content of ±2 wt.% changes the temperature and pressure estimates of ± 15 °C and ± 0.15 kbar only. Results from equations Talk2012 for the lower and upper fall deposits of the Campanian Ignimbrite eruption indicate crystallization temperatures of 919 ± 9 °C (48 pairs) and 898 ± 14 °C (40 pairs), respectively. Conversely, for the Breccia Museo eruption, we obtain crystallization temperatures of

944 ± 26 °C (48 pairs) and 970 ± 13 °C (70 pairs), respectively (Figure 9a). These estimates suggest a thermal range narrower than those reported by previous studies (Civetta et al. 1997; Fulignati et al. 2004; Marianelli et al. 2006). Moreover, within their uncertainties, these estimates agree with the crystallization temperature of about 883 °C determined through phase equilibria simulations with MELTS code (Ghiorso and Sack 1995) for the Campanian Ignimbrite magma (Fowler et al. 2007). A significant feature of the simulations is the existence of a pseudo-invariant point at 883 °C where the fraction of melt remaining in the system decreases abruptly from 0.5 to <0.1. Crystallization at this pseudo-invariant temperature leads to abrupt changes in the composition, properties (density, dissolved water content), and physical state (viscosity, volume fraction fluid) of melt, possibly setting the stage for highly explosive eruptions (Fowler et al. 2007).

Although there are no direct estimates for the magmatic pressures of the Campanian Ignimbrite, there is a general consensus that magma fractionation and differentiation occurs at shallow crustal levels (i.e., 2-6 km corresponding to 0.6-1.7 kbar; D'Antonio 2011 and references therein). Using the same clinopyroxene-liquid pairs discussed above, we have estimated the pressure conditions of both the Campanian Ignimbrite and the Breccia Museo magmas. Results from barometric equation Palk2012 indicate clinopyroxene crystallization for the lower and upper fall units of Campanian Ignimbrite at 0.58 ± 0.43 kbar and 1.27 ± 0.34 kbar, respectively; whereas, for the Breccia Museo, clinopyroxene crystallizes at 0.69 ± 0.81 kbar and 0.83 ± 0.92 kbar (Figure 9a). These pressure estimates agree with the hypothesis of differentiation at shallow crustal levels (D'Antonio 2011) and phase equilibria data, suggesting the formation of the Campanian Ignimbrite magmas at pressures lower than 3 kbar (Fowler et al. 2007).

Mt. Vesuvius

The Mt. Somma-Vesuvius is a strato-volcano consisting of a recent cone, the Vesuvius, which rises within the older Mt. Somma caldera. At present, Mt. Vesuvius is in a quiescent state characterised by fumarolic and low-magnitude seismic activity. The Mt. Somma-Vesuvius has been characterized in the past by both highly explosive subplinian and plinian eruptions alternating with small explosive/effusive activity. A total volume of 300 km^3 of magma has been erupted throughout the history of Mt. Somma-Vesuvius (Civetta and Santacroce 1992). The magmatic system produced silica undersaturated potassic to ultrapotassic rocks and consisted of multi-depth reservoirs located between 4 and 10 km, as deduced by fluid and melt inclusion data (e.g., Marianelli et al. 1999; Cioni 2000). Basalts to trachytes were produced in the oldest period of volcanism, before magmas changed from phonolitic tephrites to phonolites. The historical activity is prevalently characterized by the eruption of magma compositions ranging from leucitic tephrite to leucitic phonolite.

We have considered as input data for the new thermometer and barometer the clinopyroxene-liquid pairs from Mercato eruption (8 ka BP), Avellino eruption (3.4 ka BP) and the historical AD 79 eruption (Table 4EA). On the basis of phase equilibria experiments and in comparison with the textural and compositional features of natural products, Scaillet et al. (2008) have estimated a pre-eruptive pressure of 2 ± 0.2 kbar, and temperature of 785 ± 15 °C for both Mercato and Avellino eruptions, and 815 ± 15 °C for the 79 AD eruption. However, the crystallization temperature experimentally determined by Scaillet et al. (2008) for the AD 79 eruption is not fully consistent with data from melt and fluid inclusion studies. A large number of analyses on inclusions in phenocrysts indicate two different crystallization depths for the Vesuvius magmas at 4 km and >11 km, and temperatures of 850-900 °C and 1200 °C, respectively (e.g., Belkin et al. 1985, 1998; Cortini et al. 1985; Belkin and De Vivo 1993; Cioni et al. 1995, 1998; Marianelli et al. 1999; Cioni 2000). In particular, the 850-900 °C temperature range has been inferred for the phonolitic magma feeding the AD 79 eruption (e.g., Cioni et al., 1995). To estimate temperature and pressure of Mt. Vesuvius magmas, we have used clinopyroxene-liquid pairs reported by Aulinas et al. (2008) for the Mercato eruption, and clinopyroxene-liquid pairs reported by Cioni et al. (1998) and Balcone-Boissard et al. (2008, 2012) for the Avellino and AD 79 eruptions, respectively. For the Mercato and Avellino eruptions, equation Talk2012 yields crystallization temperatures of 800 ± 10 °C and 770 ± 14 °C (90 data from Aulinas et al. 2008, Cioni et al. 1998 and Balcone-Boissard et al. 2012) (Figure 9b), in agreement with results from phase equilibria experiments of Scaillet et al. (2008). In the case of the AD 79 eruption, the temperature predicted by equation Talk2012 is 882 ± 19 °C (24 data from Cioni et al. 1998 and Balcone-Boissard et al. 2008). This value is higher than experimental determinations of Scaillet et al. (2008), but in agreement with estimates from melt inclusion data of Cioni et al. (1995). Our new equation Palk2012 predicts clinopyroxene crystallization at pressures of 1.57 ± 1.22 kbar, 1.12 ± 0.82 kbar, and 1.86 ± 0.98 kbar for Mercato, Avellino and AD 79 eruptions, respectively (Figure 9b). The standard deviation associated with these estimates is relatively high, but however consistent with the knowledge of multi-depth reservoirs located from 4 to 10 km of depth (e.g., Belkin et al. 1985; Belkin and De Vivo 1993; Marianelli et al. 1999; Cioni 2000).

6. Conclusion

We have designed, calibrated and tested a new thermometer and a new barometer specific to alkaline differentiated magmas. These models have been calibrated through regression analyses of datasets that strictly reproduce the compositional variability of these magmas in nature. Compared to previous thermometers and barometers, the models presented in this study resulted to be

significantly more precise to estimate crystallization temperatures and pressures in alkaline differentiated magmas.

The two new models have been tested and validated by calculating the crystallization temperature and pressure of clinopyroxenes occurring in eruptive products at the Phlegrean Fields and Mt. Vesuvius, and by comparing these values with those inferred by means of melt and fluid inclusion data and phase equilibria experiments. The new thermometer and barometer here presented can be confidently used to estimate magmatic temperatures and pressures in alkaline magma reservoirs feeding highly explosive eruptions.

Acknowledgments

We are grateful to Keith D. Putirka, an anonymous reviewer and the editor Timothy L. Grove for their useful comments. Tracy Paul is acknowledged for providing experimental materials and technical supports during the experimental work. Bob Myhill is acknowledged for thoughtful input to this manuscript. A. Cavallo is acknowledged for assistance during electron microprobe analysis. This work was funded by Sapienza - Università di Roma, Istituto Nazionale di Geofisica e Vulcanologia and Depths of the Earth Company. SM was supported by ERC Starting grant 259256 GLASS project.

References

Andujar J, Costa F, Martí J, Wolff JA, Carroll MR (2008) Experimental constraints on pre-eruptive conditions of phonolitic magma from the caldera-forming El Abrigo eruption, Tenerife (Canary Islands). Chem Geol 257:173–191

Andujar J, Costa A, Marti J (2010) Magma storage conditions of the last eruption of Teide volcano (Canary Islands, Spain). Bull Volcanol 72:381-395

Andujar J, Scaillet B (2012) Experimental constraints on parameters controlling the difference in the eruptive dynamics of phonolitic magmas: The case of Tenerife (Canary islands). J Petrol 53:1777-1806

Aulinas M, Civetta L, Di Vito MA, Orsi G, Gimeno D, Fernandez-Turiel JL (2008) The “Pomici di Mercato” Plinian eruption of Somma-Vesuvius: Magma chamber processes and eruption dynamics. Bull Volcanol 70:825-840

Balcone-Boissard H, Villemant B, Boudon G, Michel A (2008) Non-volatile vs volatile behaviours of halogens during the AD 79 plinian eruption of Mt. Vesuvius, Italy. Earth Planet Sci Lett 269:66-79

Balcone-Boissard H, Boudon G, Ucciani G, Villemant B, Cioni R, Civetta L, Orsi G (2012) Magma degassing and eruption dynamics of the Avellino pumice Plinian eruption of Somma–Vesuvius (Italy). Comparison with the Pompeii eruption. Earth Planet Sci Lett 331-332:257-268

Belkin HE, De Vivo B, Roedder E, Cortini M (1985) Fluid inclusion geobarometry from ejected Mt. Somma-Vesuvius nodules. Am Mineral 70:288-303

Belkin HE, De Vivo B, Torok K, Webster JD (1998) Pre-eruptive volatile content, melt-inclusion chemistry, and microthermometry of interplinian Vesuvius lavas (pre-A.D. 1631). J Volcanol Geotherm Res 82:79-95

Belkin HE, De Vivo B (1993) Fluid inclusion studies of ejected nodules from plinian eruptions of Mt. Somma-Vesuvius. J Volcanol Geotherm Res 58:98-100

Berndt J, Holtz F, Koepke J (2001) Experimental constraints on storage conditions in the chemically zoned phonolitic magma chamber of the Laacher See volcano. Contrib Min Petrol 140:469-486

Civetta L, Orsi G, Pappalardo L, Fisher RV, Heiken G, Ort M (1997) Geochemical zoning, mingling, eruptive dynamics depositional processes -the Campanian Ignimbrite, Flegrei caldera, Italy. J Volcanol Geotherm Res 75:183-219

Civetta L, Santacroce R (1992) Steady state magma supply in the last 3400 years of Vesuvius activity. Acta Vulcanol 2:147-159

Cortini M, Lima A, De Vivo B (1985) Trapping temperatures of melt inclusions from ejected vesuvian mafic xenoliths. J Volcanol Geotherm Res 26:167-172

Cioni R (2000) Volatile content and degassing processes in the A.D. 79 magma chamber at Vesuvius (Italy). Contrib Mineral Petrol 140:40-54

Cioni R, Civetta L, Marianelli P, Metrich N, Santacroce R, Sbrana A (1995) Compositional layering and syn-eruptive mixing of periodically refilled shallow magma chamber: the A.D. 79 Plinian eruption of Vesuvius. J Petrol 36:739–776

Cioni R, Longo A, Macedonio G, Santacroce R, Sbrana A, Sulpizio R, Andronico D (2003) Assessing pyroclastic fall hazard through field data and numerical simulations: Example from Vesuvius. J Geophys Res 108(B2) doi:10.1029/2001JB000642

Cioni R, Marianelli P, Santacroce R (1998) Thermal and compositional evolution of the shallow magma chambers of Vesuvius, evidence from pyroxene phenocrysts and melt inclusions. J Geophys Res 103:18277-1829

Conte AM, Dolfi D, Gaeta M, Misiti V, Mollo S, Perinelli C (2009) Experimental constraints on evolution of leucite–basanite magma at 1 and 10–4 GPa: implications for parental compositions of Roman high-potassium magmas. Eur J Min 214:763-782

D'Antonio (2011) Lithology of the basement underlying the Campi Flegrei caldera: Volcanological and petrological constraints. J Volcanol Geotherm Res 200:91-98

De Astis G, La Volpe L, Peccerillo A, Civetta L (1997) Volcanological and petrological evolution of Vulcano island (Aeolian Arc, southern Tyrrhenian Sea). J Geophys Res 102:8021-8050

Del Gaudio P, Mollo S,Ventura G, Iezzi G, Taddeucci I, Cavallo A (2010) Cooling rate-induced differentiation in anhydrous and hydrous basalts at 500 MPa: Implications for the storage and transport of magmas in dikes. Chem Geol 270:164-178

Devine JD, Gardner JE, Brack HP, Layne GD, Rutherford MJ (1995) Comparison of microanalytical methods for estimating H_2O contents of silicic volcanic glasses. Am Min 80:319-328

Esposti Ongaro T, Papale P, Neri A, Del Seppia D (2006) Influence of carbon dioxide on the large-scale dynamics of magmatic eruptions at Phlegrean Fields (Italy), Geophys Res Lett 33:L06318

Fabbrizio A, Carroll MR (2008) Experimental constraints on the differentiation process and pre-eruptive conditions in the magmatic system of Phlegraean Fields (Naples, Italy). J Volcanol Geotherm Res 171:88-102

Fedele L, Zanetti A, Morra V, Lustrino M, Melluso L, Vannucci R (2009) Clinopyroxene/liquid trace element partitioning in natural trachyte–trachyphonolite systems: insights from Campi Flegrei (southern Italy). Contrib Mineral Petrol 158:337-356

Fontijn K, Ernst GGJ, Elburg MA, Williamson D, Abdallah E, Kwelwa S, Mbede E, Jacobs P (2010) Holocene explosive eruptions in the Rungwe Volcanic Province, Tanzania. J Volcanol Geotherm Res 196:91-110

Fowler SJ, Spera F, Bohrson W, Belkin HE, De Vivo B (2007) Phase equilibria constraints on the chemical and physical evolution of the Campanian Ignimbrite. J Petrol 48:459-493

Freda C, Gaeta M, Palladino DM, Trigila R (1997) The Villa Senni Eruption (Alban Hills, central Italy): the role of H_2O and CO_2 on the magma chamber evolution and on the eruptive scenario. J Volcanol Geotherm Res 78:103-120

Freda C, Gaeta M, Misiti V, Mollo S, Dolfi D, Scarlato P (2008) Magma–carbonate interaction: an experimental study on ultrapotassic rocks from Alban Hills (Central Italy). Lithos 101:397-415

Fulignati P, Marianelli P, Proto M, Sbrana A (2004) Evidences for disruption of a crystallizing front in a magma chamber during caldera collapse: an example from the Breccia Museo unit (Campanian Ignimbrite eruption, Italy). J Volcanol Geotherm Res 133:141-155

Ghiorso MS, Sack RO (1995) Chemical mass transfer in magmatic processes. IV. A revised and internally consistent thermodynamic model for the interpolation and extrapolation of liquid-solid

equilibria in magmatic systems at elevated temperatures and pressures. Contrib Mineral Petrol 119:197–212

Jefferys WH, Berger JO (1992) Ockham's razor and Bayesian analysis. Am J Sci 80:64-72

Lindsley DH (1983) Pyroxene thermometry. Am Mineral 68, 477-493

Marianelli P, Métrich N, Sbrana A (1999) Shallow and deep reservoirs involved in magma supply of the 1944 eruption of Vesuvius. Bull Volcanol 61:48-63

Marianelli P, Sbrana A, Proto M (2006) Magma chamber of the Campi Flegrei supervolcano at the time of eruption of the Campanian Ignimbrite. Geology 34:937–940

Masotta M, Freda C, Gaeta M (2012a) Origin of crystal-poor, differentiated magmas: insights from thermal gradient experiments. Contrib Min Petrol 163:49-65

Masotta M, Freda C, Paul TA, Moore GM, Gaeta M., Scarlato P, Troll V (2012b) Low pressure experiments in piston cylinder apparatus: Calibration of newly designed 25 mm furnace assemblies to P=150 MPa. Chem Geol 312-313:74-79

Masotta M, Gaeta M, Gozzi F, Marra F, Palladino DM, Sottili G (2010) H_2O- and temperature-zoning in magma chambers: the example of the Tufo Giallo della Via Tiberina eruptions (Sabatini Volcanic District, central Italy). Lithos 118:119–130

Mollo S, Gaeta M, Freda C, Di Rocco T, Misiti V, Scarlato P (2010a) Carbonate assimilation in magmas: A reappraisal based on experimental petrology. Lithos 114:503-514

Mollo S, Del Gaudio P, Ventura G, Iezzi G, Scarlato P (2010b) Dependence of clinopyroxene composition on cooling rate in basaltic magmas: Implications for thermobarometry. Lithos, 118:302-312

Mollo S, Lanzafame G, Masotta M, Iezzi G, Ferlito C, Scarlato P (2011) Cooling history of a dike as revealed by mineral chemistry: A case study from Mt. Etna volcano. Chem Geol 283:261-273

Mollo S, Misiti V, Scarlato P, Soligo M (2012) The role of cooling rate in the origin of high temperature phases at the chilled margin of magmatic intrusions. Chem Geol 322-323:28-46

Mollo S, Putirka K, Iezzi G, Scarlato P (2013a), The control of cooling rate on titanomagnetite composition: Implications for a geospeedometry model applicable to alkaline rocks from Mt. Etna volcano. Contrib Mineral Petrol 165:457–475

Mollo S, Putirka K, Misiti V, Soligo M, Scarlato P (2013b), A new test for equilibrium based on clinopyroxene-melt pairs: Clues on the solidification temperatures of Etnean alkaline melts at post-eruptive conditions. Chemical Geology doi: http://dx.doi.org/10.1016/j.chemgeo.2013.05.026

Nimis P (1995) A clinopyroxene geobarometer for basaltic systems based on crystals-structure modeling. Contrib Mineral Petrol 121:115-125

Nimis P, Taylor WR (2000) Single clinopyroxene thermobarometry for garnet peridotites. Part 1 Calibration and testing of a Cr-in-cpx barometer and an enstatite-in-cpx thermometer. Contrib Mineral Petrol 139:541-554

Nimis P, Ulmer P (1998) Clinopyroxene geobarometry of magmatic rocks. Part 1: an expanded structural geobarometer for anhydrous and hydrous basic and ultrabasic systems. Contrib Mineral Petrol 133:122-135

Orsi G, Civetta L, Del Gaudio C, de Vita S, Di Vito RA, Isaia R, Petrazzuoli SM, Ricciardi GP, Ricco C (1999) Short-term ground deformations and seismicity in the resurgent Campi Flegrei caldera (Italy): an example of active block-resurgence in a densely populated area. J Volcanol Geotherm Res 91:415-451

Pabst S, Wörner G, Civetta L, Tesoro R (2008) Magma chamber evolution prior to the Campanian Ignimbrite and Neapolitan Yellow Tuff eruptions (Phlegrean Fields, Italy). Bull Volcanol 70:961-976

Papale P, Moretti R, Barbato D (2006) The compositional dependence of the saturation surface of $H_2O + CO_2$ fluids in silicate melts. Chem Geol 229:78-95

Putirka K (1999) Clinopyroxene+liquid equilibrium to 100 kbar and 2450 K. Contrib Mineral Petrol 135:151-163

Putirka KD (2008) Thermometers and barometers for volcanic systems. In: Putirka KD, Tepley F (Eds) Minerals, inclusions, and volcanic processes: reviews in mineralogy and geochemistry, vol 69. pp 61–120

Putirka K, Johnson M, Kinzler R, Walker D (1996) Thermobarometry of mafic igneous rocks based on clinopyroxene-liquid equilibria, 0-30 kbar. Contrib Mineral Petrol 123:92-108

Putirka K, Ryerson FJ, Mikaelian H (2003) New igneous thermobarometers for mafic and evolved lava compositions, based on clinopyroxene + liquid equilibria. Am Min 88:1542-1554

Ratkowsky DA (1990) Handbook of non-linear regression models. Marcel Decker Inc., New York

Scaillet B, Pichavant M, Cioni R (2008) Upward migration of Vesuvius magma chamber over the past 20,000 years. Nature 455:216-219

Signorelli S, Vaggelli G, Francalanci L, Rosi M (1999) Origin of magmas feeding the Plinian phase of the Campanian Ignimbrite eruption, Phlegrean Fields (Italy): constraints based on matrix-glass and glass-inclusion compositions. J Volcanol Geotherm Res 91:199-220

Todesco M, Neri A, Esposti Ongaro T, Papale P, Rosi M (2006) Pyroclastic flow dynamics and hazard in a caldera setting: Application to Phlegrean Fields (Italy). Geochem Geophys Geosystems 7:1525-2027

White JC, Espejel-Garcia VV, Anthony EY, Omenda PA (2012) Open system evolution of peralkaline trachyte and phonolite from the Suswa volcano, Kenya rift. Lithos 152:84-104

Zollo A, Judenherc S, Auger E, D'Auria L, Virieux J, Capuano P, Chiarabba C, de Franco R, Makris J, Nichelini A, Musacchio G (2003) Evidence for the buried rim of Campi Flegrei caldera from 3-d active seismic imaging. Geophys Res Lett 30(19):SDE10.1–SDE10.4

Figure Captions

Figure 1. Total alkali versus silica (TAS) diagram of experimental glasses from the alkaline dataset.

Figure 2. FE-SEM pictures showing textural features of phase equilibria experiments performed in this study.

Figure 3. Comparison between the T-sensitive $K_D(Fe\text{-}Mg)^{cpx\text{-}liq}$ model of Putirka (2008) and the new model proposed in this study for alkaline differentiated magmas.

Figure 4. Previous thermometric equations of Putirka et al. (1996) and Putirka (2008) are compared with those recalibrated in this study. Models T1, T2, T3 and T4 systematically overestimate crystallization temperatures of experimental dataset. Equation 33 shows the highest precision, although it overestimates the temperature below 850 °C. Among the recalibrated models, equation Talk33 shows the highest coefficient of determination (R^2) and the lowest standard error of estimate (SEE).

Figure 5. Previous barometric equations of Putirka et al. (1996) and Putirka (2008) are compared with those recalibrated in this study. Models P1 and P2 systematically underestimate crystallization pressures of the experimental dataset, whereas equation 32c yields a better precision. All the recalibrated equations show rather similar coefficient of determination (R^2) and standard error of estimate (SEE).

Figure 6. The new thermometer (Equation Talk2012) and barometer (Equation Palk2012) show the best prediction of crystallization temperatures and pressures of the dataset, yielding the highest coefficient of determination (R^2) and lowest the standard error of estimate (SEE).

Figure 7. Equations Talk2012 and Palk2012 were recalibrated by subtracting about 25% of clinopyroxene-liquid pairs from their calibration datasets. This population was then used as test-

data for the thermometer (20 pairs) and barometer (35 pairs). Temperature and pressure estimates for the test population are comparable to those predicted by equations Talk2012 and Palk2012.

Figure 8. Results from tests conducted using clinopyroxene compositions coexisting with tephritic phonolite and phonolitic tephrite melts from Freda et al. (1997, 2008), Conte et al. (2009), and Mollo et al. (2010a, 2010b). Equation Talk2012 does not show improvements with respect to equation 33 of Putirka (2008) when used to predict crystallization temperature of more primitive alkaline compositions not incorporated in the dataset. Conversely, the pressure prediction of equation Palk2012 is slightly better than that of equation 32c of Putirka (2008).

Figure 9. Clinopyroxene-liquid pairs from the Phlegrean Fields and Vesuvius eruptions have been used as input data for our new Equations Talk2012 (a) and Palk2012 (b). Temperature and pressure estimates agree with those determined by melt and fluid inclusion data, and phase equilibria studies. Data yielding negative pressure estimates are not reported in figure.

Figure 1
Click here to download high resolution image

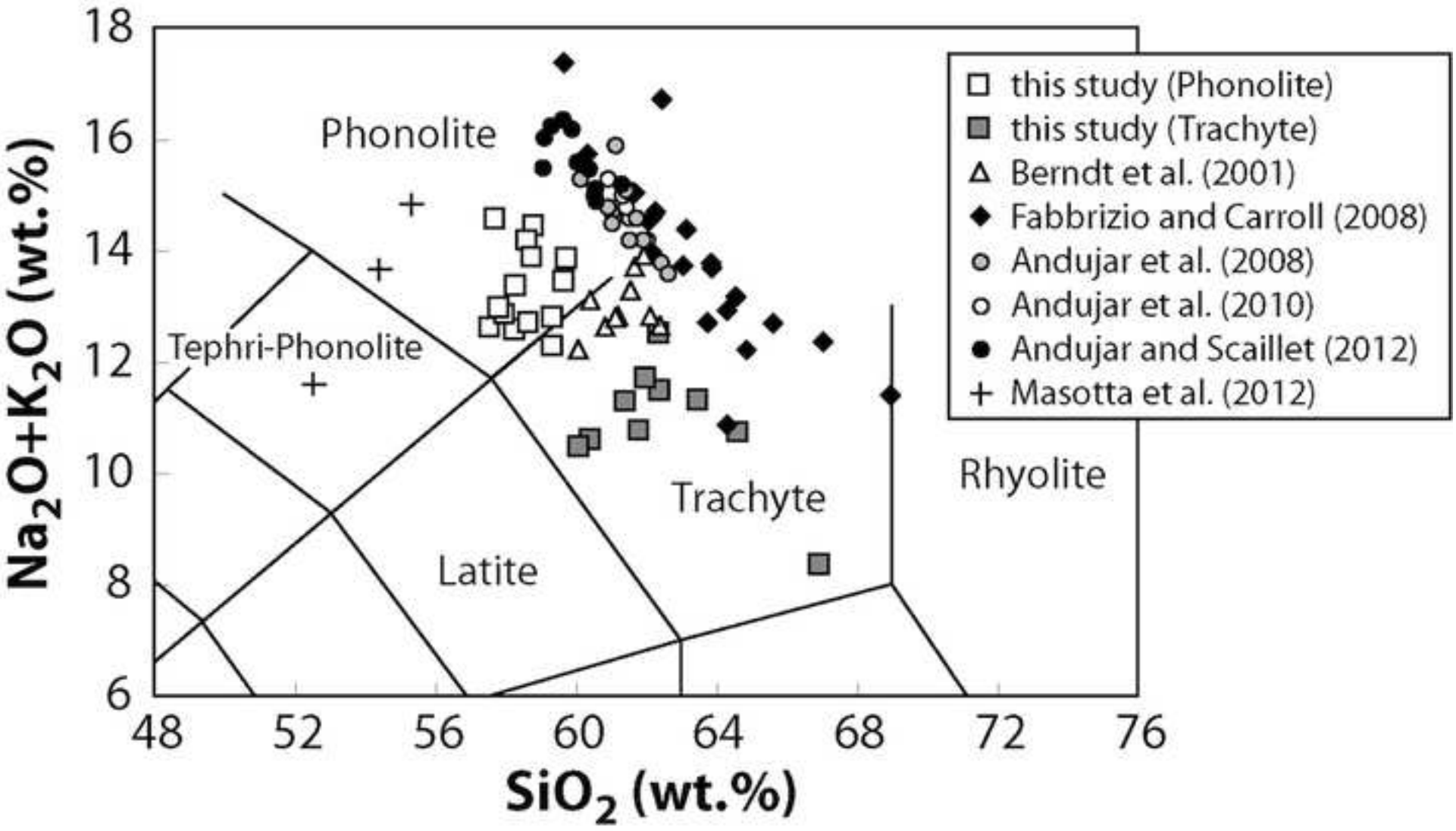

Figure 2
Click here to download high resolution image

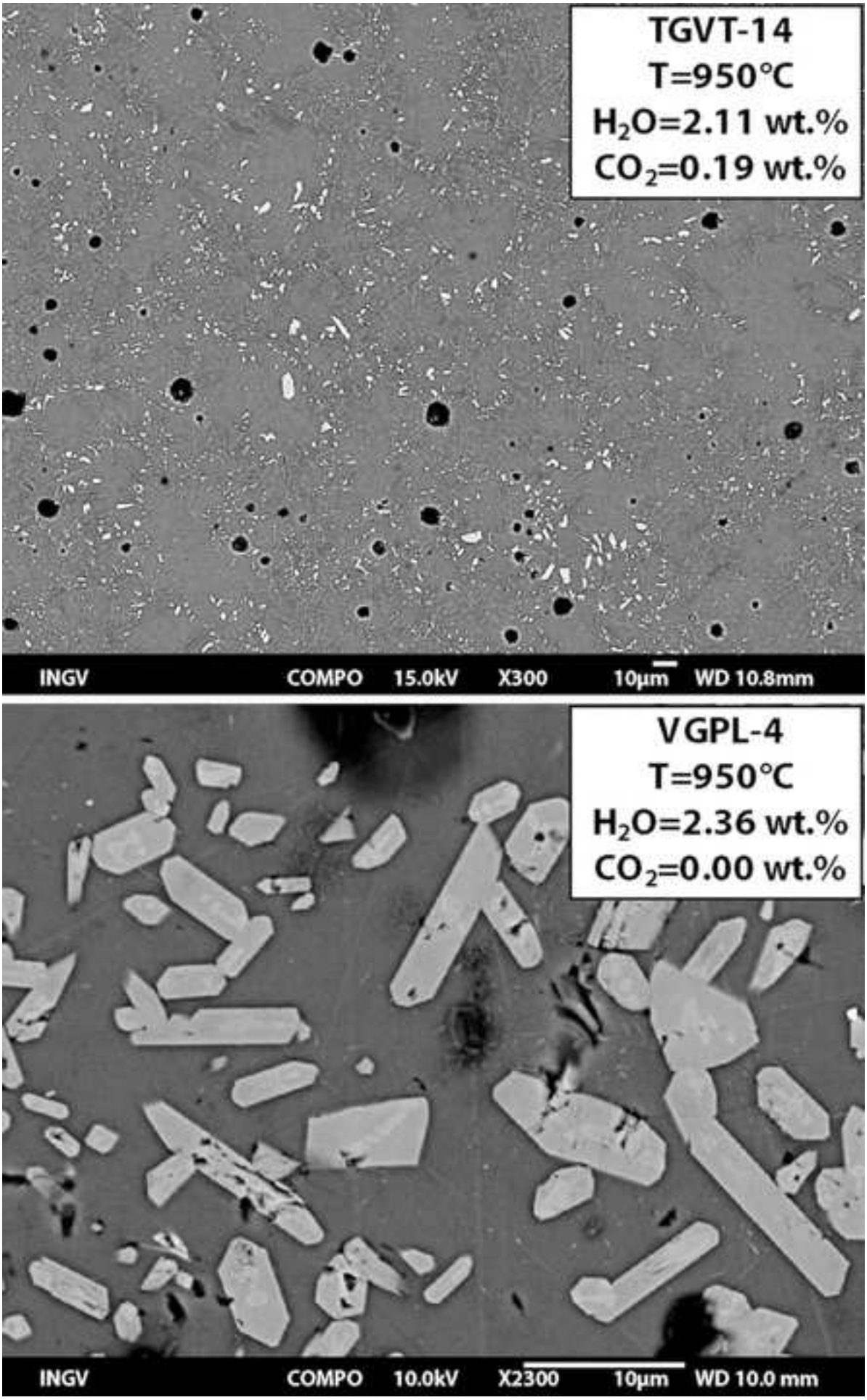

Figure 3
Click here to download high resolution image

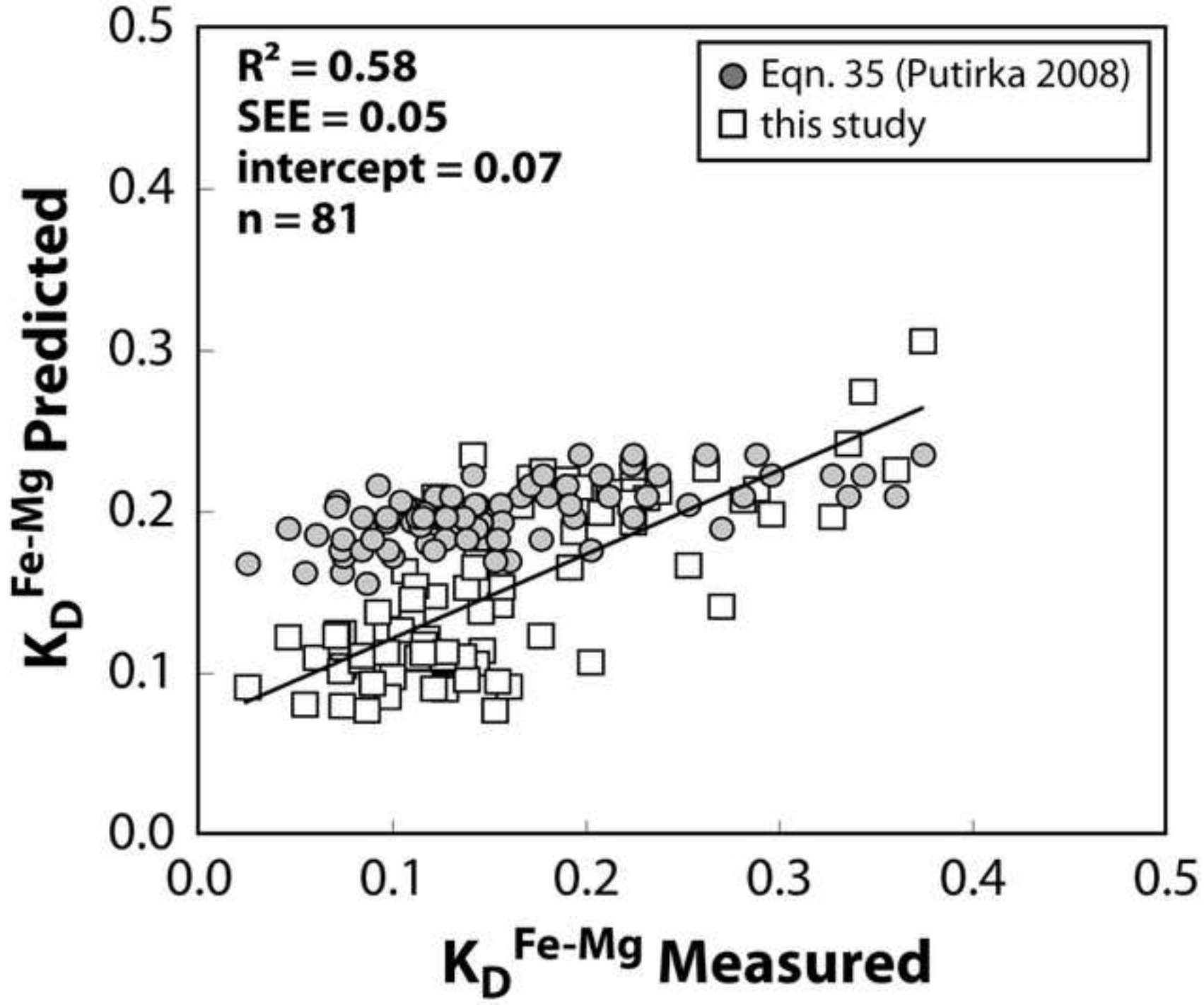

Figure 4
Click here to download high resolution image

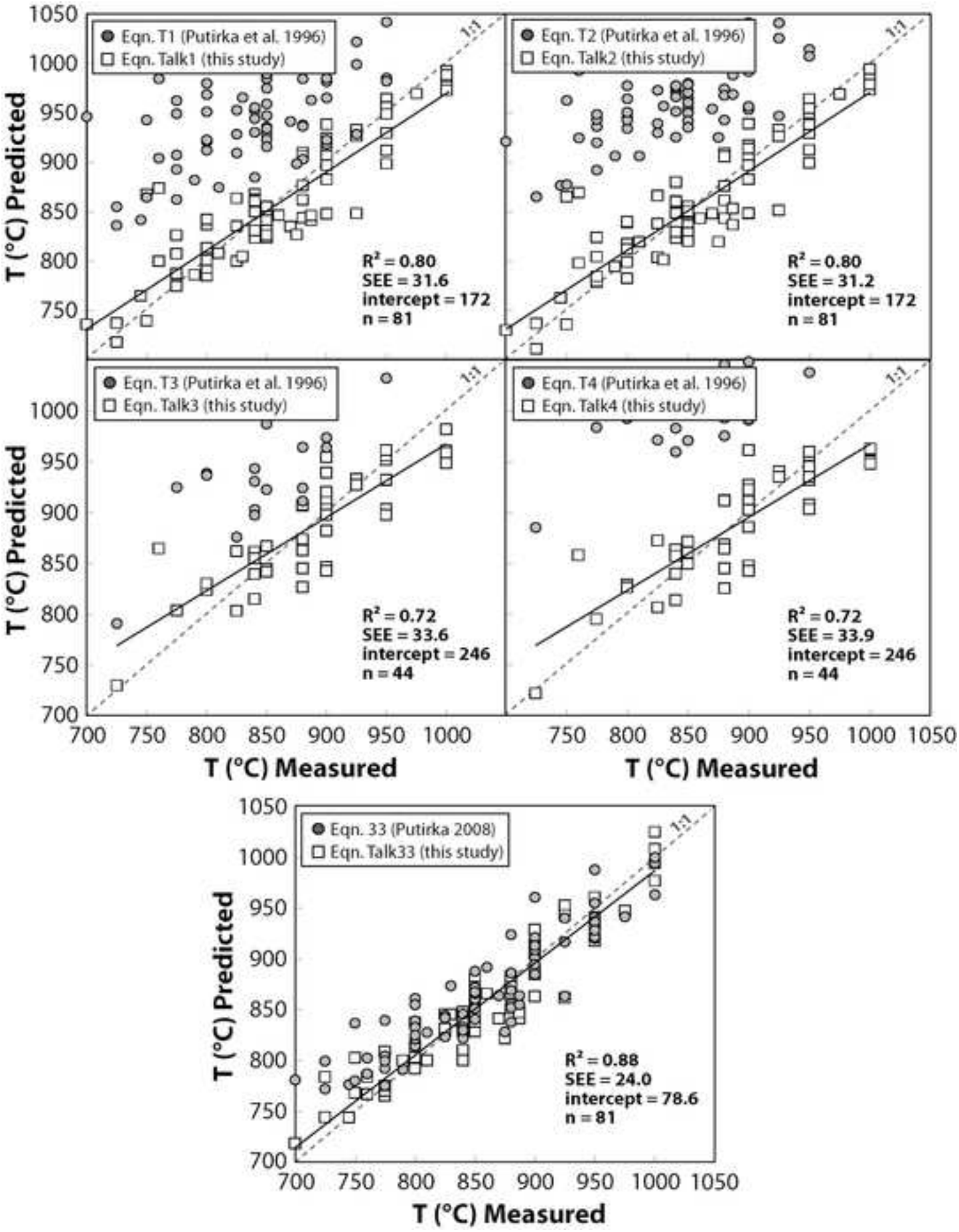

Figure 5
Click here to download high resolution image

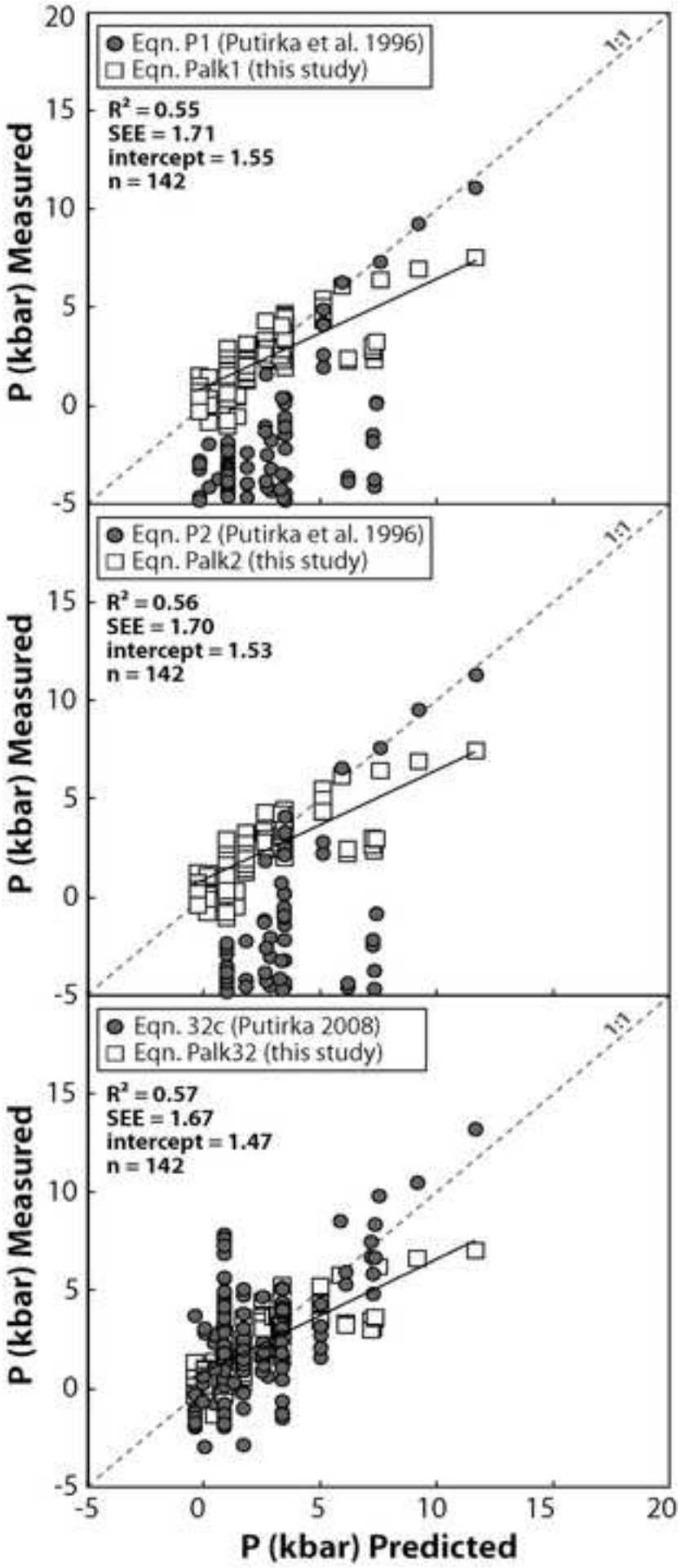

Figure 6
Click here to download high resolution image

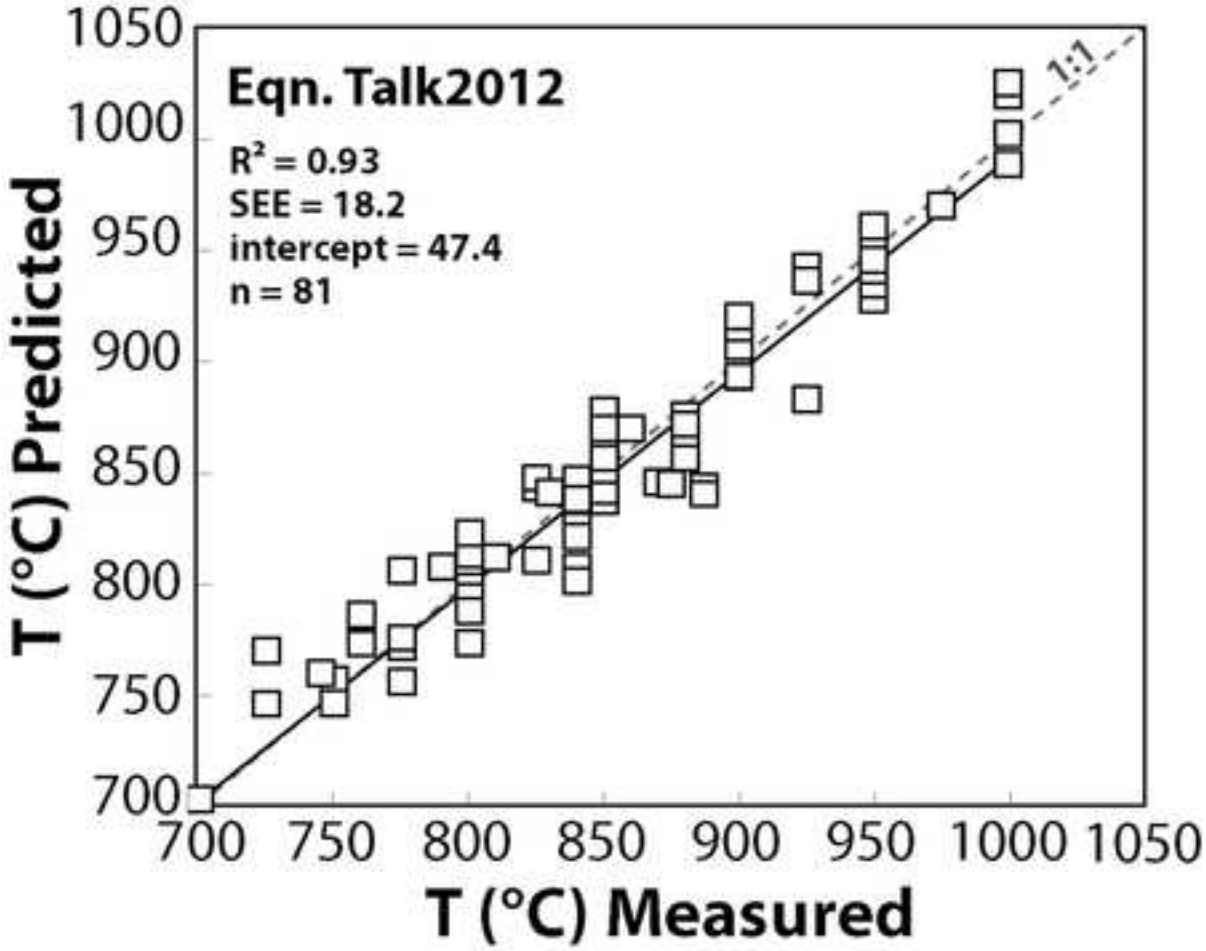

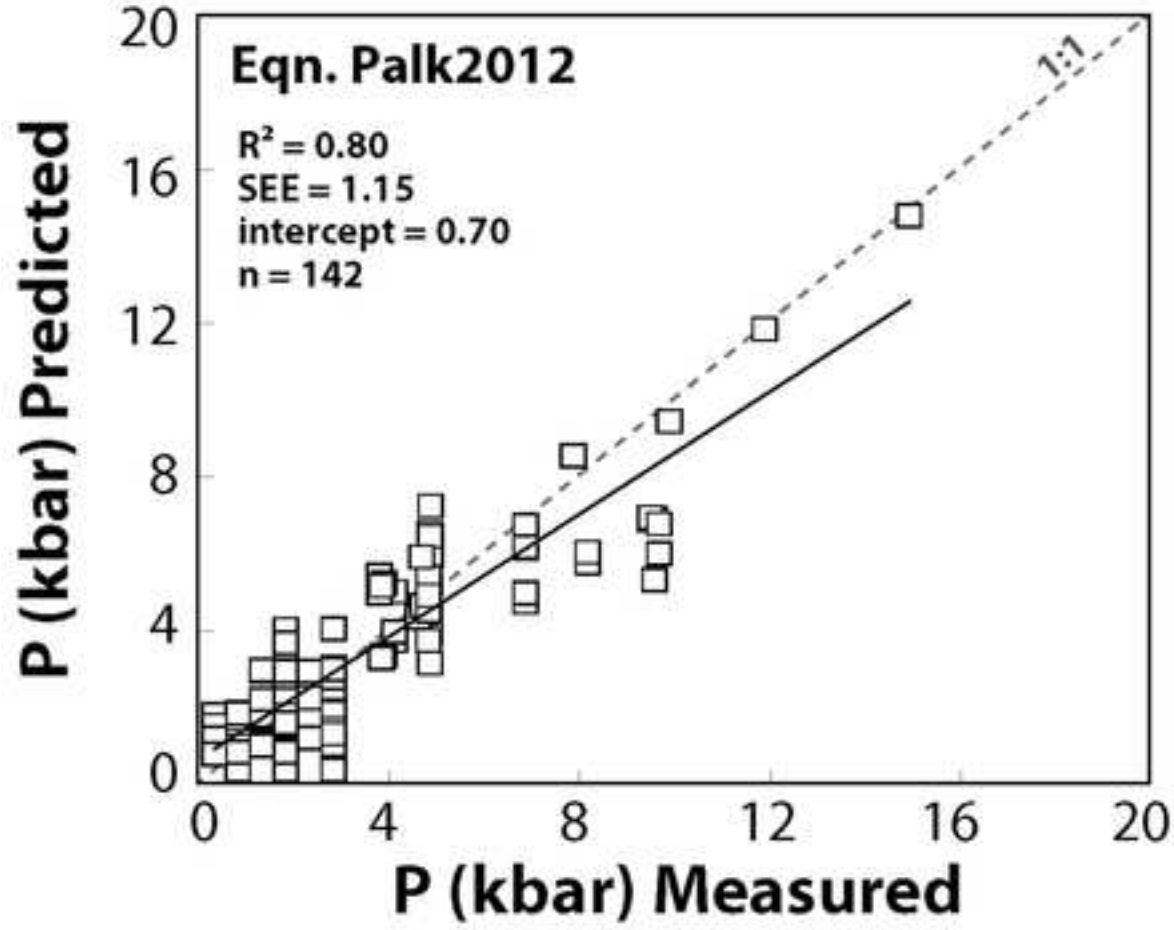

Figure 7
Click here to download high resolution image

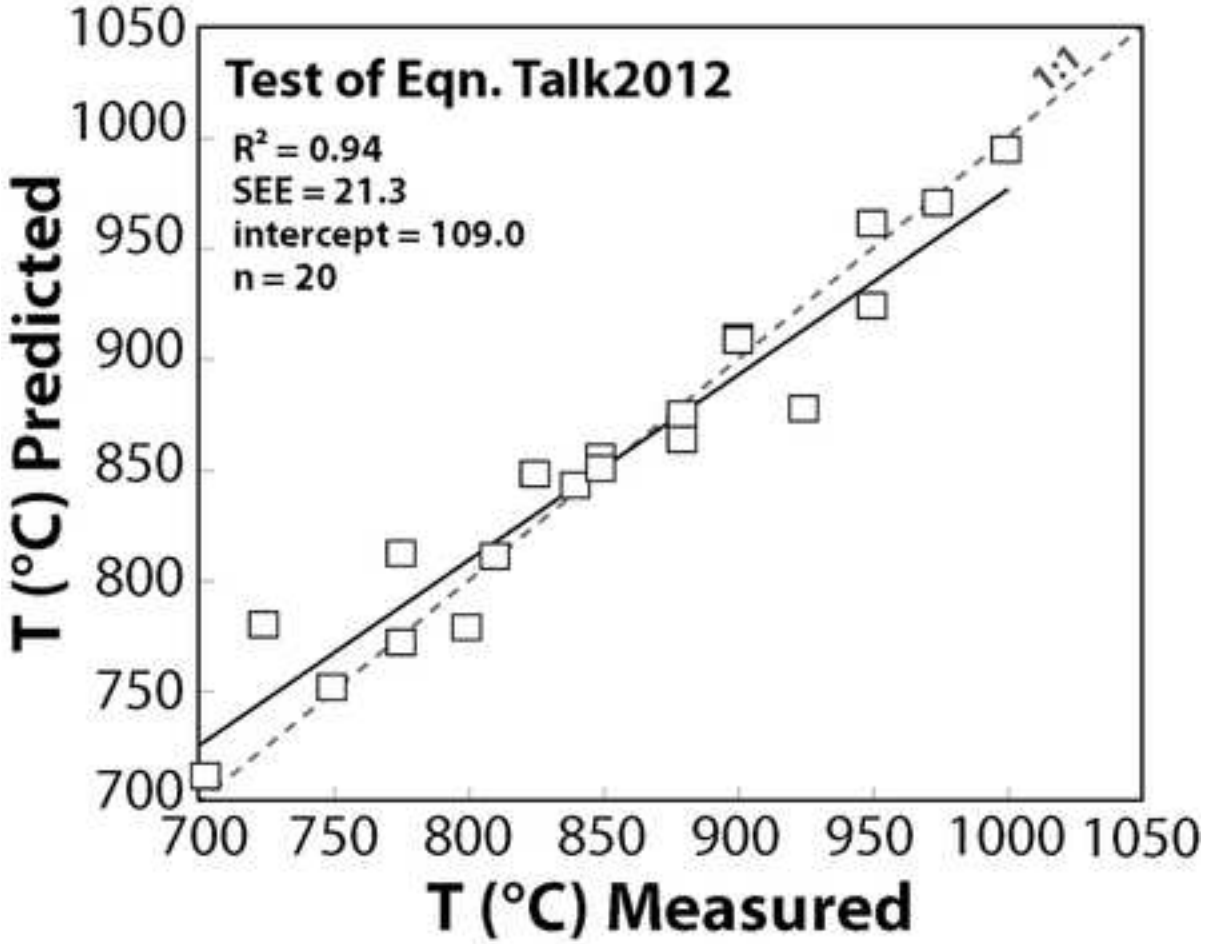

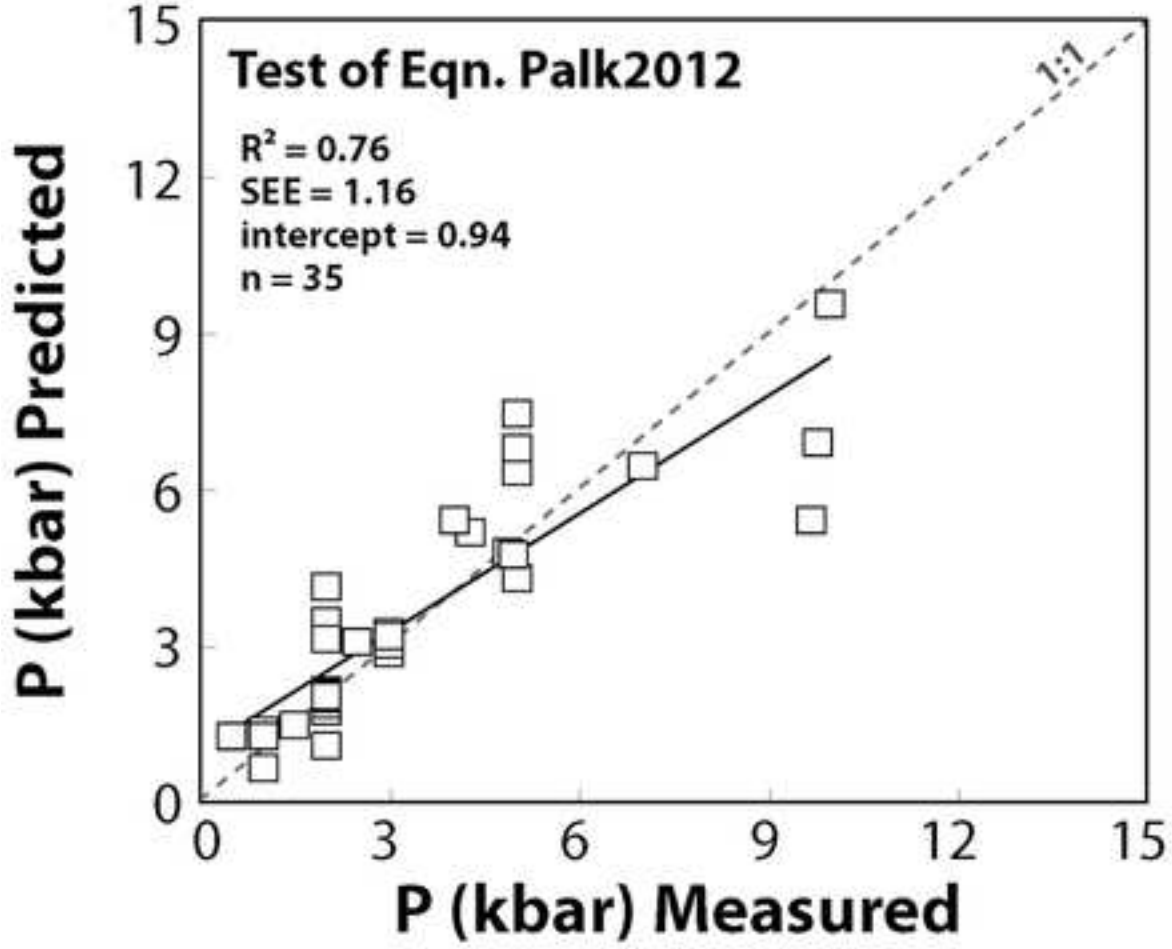

Figure 8
Click here to download high resolution image

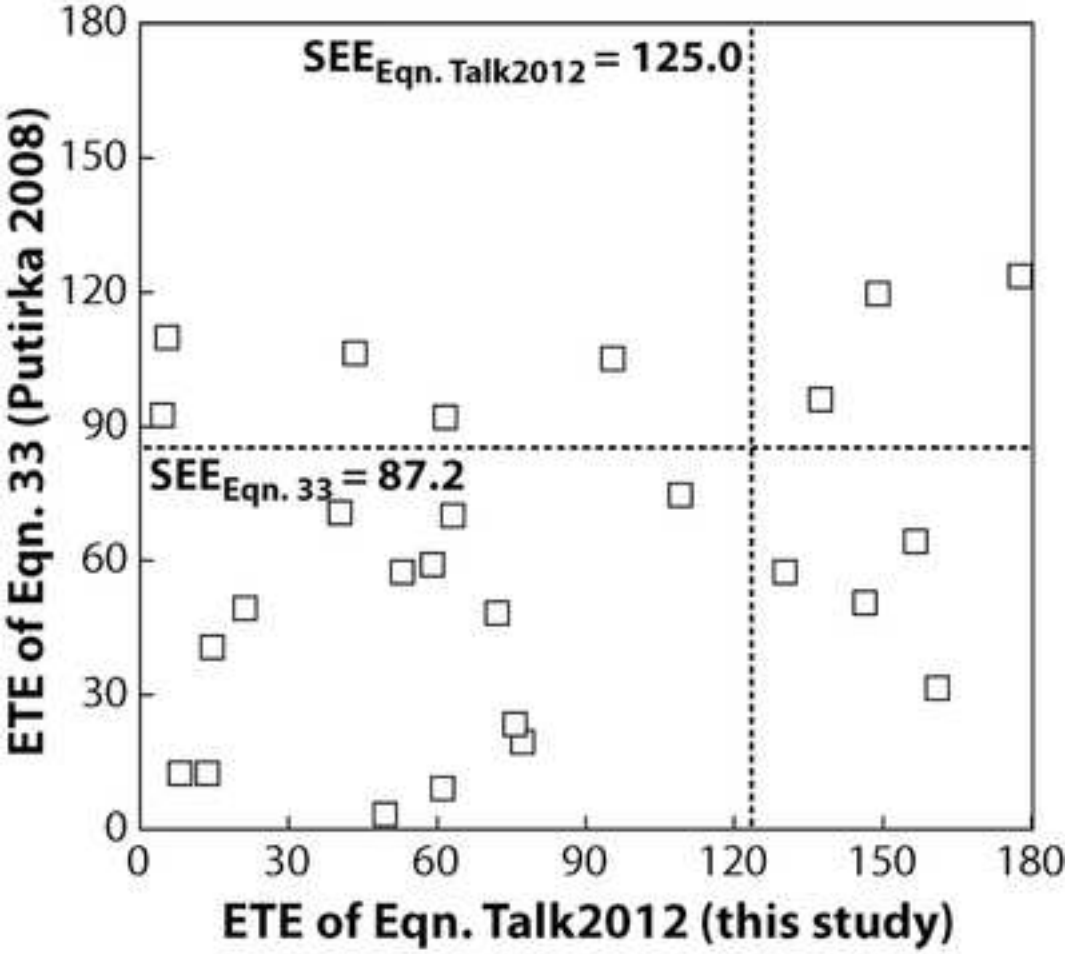

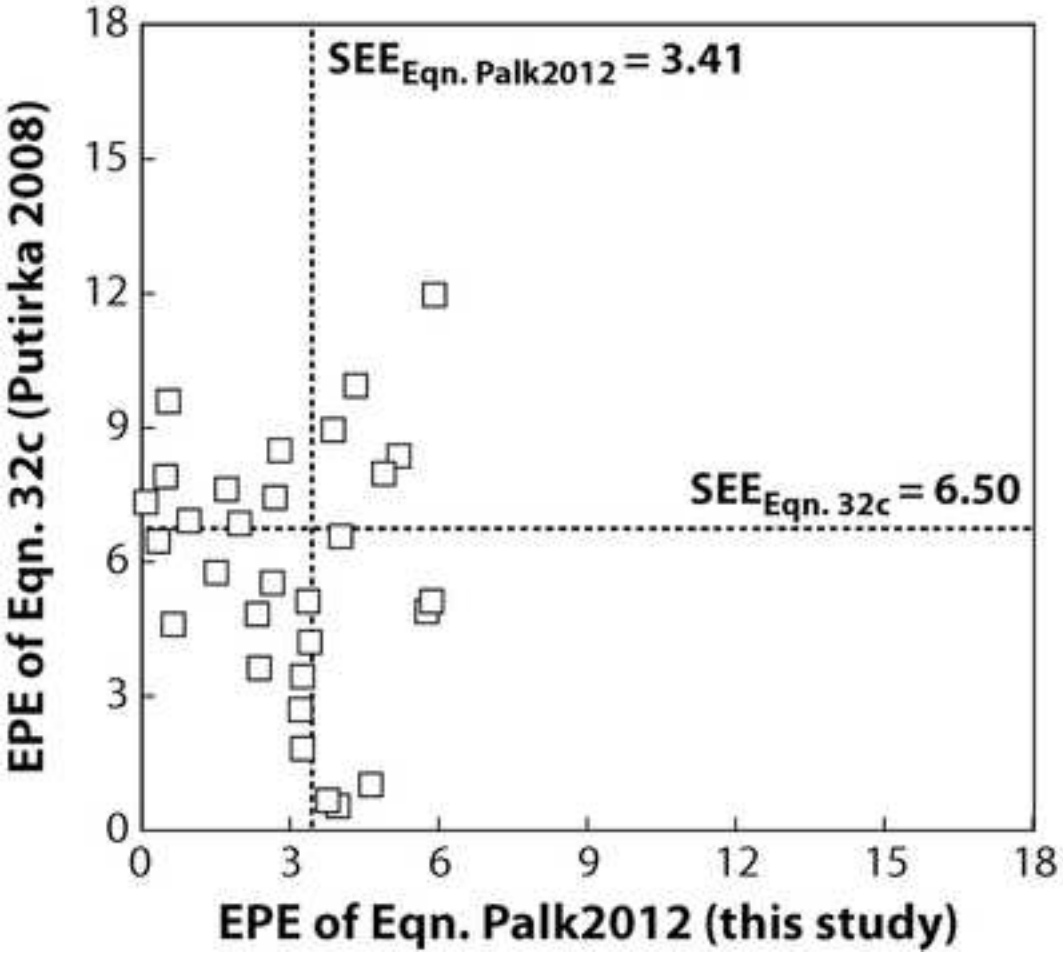

Figure 9
Click here to download high resolution image

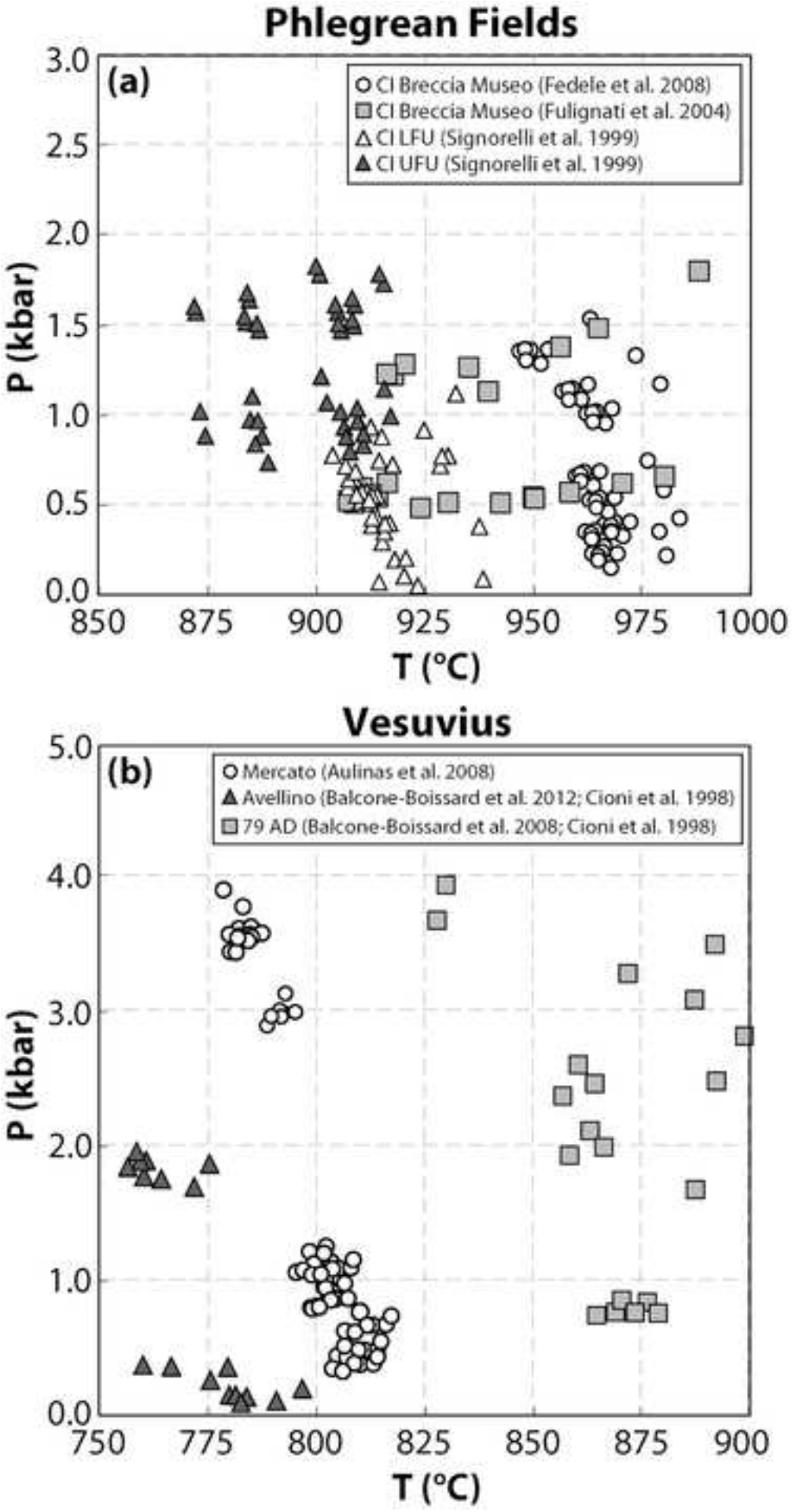

table 1
Click here to download table: Table 1.doc

Table 1. List of the starting materials of phase equilibria experiments incorporated into the dataset used to calibrate the thermometer. Tr = trachyte. Pho = phonolite. Te-Pho = tephriphonolite

Reference	This study	This study	Berndt et al. (2001)	Berndt et al. (2001)	Fabbrizio and Carroll (2008)	Fabbrizio and Carroll (2008)	Andujar et al. (2008)	Andujar et al. (2010)	Andujar and Scaillet (2012)	Masotta et al. (2012)
Starting material	TGVT - Glass	VGPL - Glass	1060 ULST - Glass	1088 ULST - Glass	Breccia Museo - Obsidian	Breccia Museo - Pumice	El Abrigo - Pumice	Lavas Negras - Glass	Montaña Blanca - Glass	SVD-0 - Glass
	Pho	Tr	Pho	Pho	Tr	Tr	Pho	Pho	Pho	Te-Pho
SiO_2	56.39	58.66	58.89	58.06	62.18	60.36	60.30	59.40	59.70	50.84
TiO_2	0.54	0.50	0.76	0.98	0.45	0.41	0.66	0.81	0.64	0.68
Al_2O_3	20.45	16.15	19.87	19.66	18.70	19.09	19.24	19.25	19.60	18.97
FeO*	2.86	5.73	3.25	3.58	3.19	3.29	2.91	3.90	3.40	7.91
MnO	0.16	0.10	0.21	0.15	0.27	0.15	0.23	0.16	0.25	0.17
MgO	0.78	2.73	0.69	0.90	0.23	1.12	0.25	0.52	0.33	2.31
CaO	5.64	5.30	3.90	4.87	1.65	2.45	0.64	1.20	0.72	8.11
Na_2O	4.64	4.39	5.34	5.02	6.16	3.81	10.10	9.18	9.63	2.62
K_2O	8.39	5.88	7.10	6.77	7.14	9.09	5.59	5.20	5.74	7.93
P_2O_5	0.16	0.26	-	-	0.02	0.22	0.06	-	-	0.46
sum	99.59	99.70	-	-	99.25	99.23	99.40	100.70	100.01	99.59
Na_2O/K_2O	0.55	0.75	0.75	0.74	0.86	0.42	1.81	1.77	1.68	0.33

** Total iron reported as FeO*

table 2
Click here to download table: Table 2.doc

Table 2. List of the phase equilibria experiments conducted at 2 kbar. Liq = liquid. Cpx = clinopyroxene. Fsp = feldspar.

Run	T (°C)	H_2O^a	CO_2^b	H_2O^c	CO_2^d	Phase assemblage
Phonolite (Tufo Giallo della Via Tiberina)						
TGVT-1	850	3.00	0.00	5.15	0.00	Liq+Cpx+Fsp
TGVT-2	850	1.50	0.00	5.05	0.00	Liq+Cpx+Fsp
TGVT-3	900	2.89	0.00	3.52	0.00	Liq+Cpx+Fsp
TGVT-4	900	2.12	0.00	2.66	0.00	Liq+Cpx+Fsp
TGVT-5	900	3.89	0.17	5.39	0.06	Liq+Cpx+Fsp
TGVT-6	900	3.93	0.40	3.54	0.07	Liq+Cpx+Fsp
TGVT-7	900	3.92	0.00	4.05	0.00	Liq+Cpx+Fsp
TGVT-8	900	2.63	0.11	4.29	0.08	Liq+Cpx+Fsp
TGVT-9	900	2.92	0.35	3.62	0.07	Liq+Cpx+Fsp
TGVT-10	925	2.47	0.00	2.80	0.00	Liq+Cpx+Fsp
TGVT-11	925	5.36	0.00	5.43	0.00	Liq
TGVT-12	925	3.31	0.27	3.31	0.06	Liq+Cpx+Fsp
TGVT-13	950	3.40	0.21	2.29	0.09	Liq+Cpx+Fsp
TGVT-14	950	2.11	0.19	3.44	0.11	Liq+Cpx+Fsp
Trachite (Grotte dei Palizzi)						
VGPL-1	1000	2.89	0.00	3.29	0.00	Liq+Cpx
VGPL-2	900	3.50	0.22	5.00	0.10	Liq+Cpx+Fsp
VGPL-3	950	4.74	0.00	6.84	0.00	Liq+Cpx
VGPL-4	950	2.36	0.00	4.51	0.00	Liq+Cpx+Fsp
VGPL-5	950	2.96	0.14	2.45	0.05	Liq+Cpx+Fsp
VGPL-6	950	2.81	0.19	3.04	0.07	Liq+Cpx+Fsp
VGPL-7	975	4.08	0.00	6.21	0.00	Liq+Cpx
VGPL-8	1000	3.52	0.17	4.64	0.07	Liq+Cpx
VGPL-9	1000	2.50	0.24	1.77	0.04	Liq+Cpx
VGPL-10	1000	3.39	0.00	3.40	0.00	Liq+Cpx

[a] Initial H_2O concentration
[b] Initial CO_2 concentration
[c] H_2O measured "by difference" (Devine et al. 1995)
[d] CO_2 determined by H_2O-CO_2 solubility model of Papale et al. (2006)

table 3
Click here to download table: Table 3.doc

Table 3. Regression parameters from thermometers and barometers of Putirka et al. (1996) and Putirka (2008) are compared with those from this study. R^2 = coefficient of determination. SEE = Standard error of estimate.

	a	b	c	d	e	f	g	h	i	SEE	R^2
Thermometric equations of Putirka et al. (1996) and Putirka (2008)											
Eqn. T1	6.73	-0.26	-0.86	0.52						119.6	0.59
Eqn. T2	6.59	-0.16	-0.65	0.23	-0.02					126.9	0.71
Eqn. T3	6.92	-0.18	-0.84	-0.29						145.4	0.68
Eqn. T4	7.20	-0.04	-0.59	-0.18	-0.03					154.0	0.67
Eqn. 33	7.53	-0.14	0.07	-14.90	-0.08	-3.62	-1.10	-0.18	-0.027	31.4	0.80
Recalibrated thermometric equations of Putirka et al. (1996) and Putirka (2008)											
Eqn. Talk1	6.74	-0.02	-0.69	-0.15						31.6	0.80
Eqn. Talk2	6.52	-0.04	-0.68	-0.15	0.08					31.2	0.80
Eqn. Talk3	5.05	-0.06	-0.81	0.68						33.6	0.74
Eqn. Talk4	3.85	-0.06	-0.87	0.91	0.19					33.9	0.74
Eqn. Talk33	6.81	0.003	0.05	-25.04	-0.30	2.25	-1.91	-0.02	0.06	24.0	0.88
Barometric equations of Putirka et al. (1996) and Putirka (2008)											
Eqn. P1	-54.3	299	36.4	367						7.29	0.46
Eqn. P2	-50.7	394	36.4	20.0						9.54	0.53
Eqn. 32c	-57.9	0.048	40.6	-47.7	0.676	-153	6.89			2.94	0.32
Recalibrated barometric equations of Putirka et al. (1996) and Putirka (2008)											
Eqn. Palk1	-8.84	79.0	11.6	8.60						1.71	0.55
Eqn. Palk2	-6.28	38.2	9.42	6.16						1.70	0.56
Eqn. Palk32c	-16.3	0.014	-12.4	-9.19	0.21	38.7	1.59			1.67	0.57

table 4
Click here to download table: Table 4.doc

Table 4. Major elements and components of clinopyroxenes from phase equilibria experiments performed in this study. sd = standard deviation calculated for the number of analyses in parenthesis.

Run	SiO_2	TiO_2	Al_2O_3	FeO	MnO	MgO	CaO	Na_2O	K_2O	P_2O_5	Total	DiHd	EnFs	Jd	CaTs	CaTi	mg-*number*	Kd(Fe-Mg)
Phonolite (Tufo Giallo della Via Tiberina)																		
TGVT-1	41.70	1.64	9.73	14.28	0.52	6.19	22.08	0.45	0.23	0.11	96.93	0.740	0.057	0.035	0.107	0.106	0.30	0.19
sd(7)	0.15	0.42	1.54	0.55	0.04	0.48	0.24	0.14	0.11	0.06								
TGVT-2	41.96	2.29	8.72	16.63	0.73	4.84	21.68	0.82	0.30	0.03	98.00	0.762	0.045	0.064	0.043	0.132	0.23	0.23
sd(3)	1.06	0.35	1.21	0.43	0.06	0.28	0.28	0.09	0.09	0.03								
TGVT-3	43.74	2.16	8.36	12.44	0.45	7.50	22.57	0.49	0.22	0.01	97.94	0.778	0.037	0.038	0.074	0.101	0.38	0.12
sd(9)	0.99	0.50	0.93	0.15	0.01	0.44	0.39	0.02	0.02	0.02								
TGVT-4	43.86	1.54	9.27	13.15	0.51	7.16	22.60	0.59	0.33	0.00	99.00	0.755	0.046	0.044	0.097	0.095	0.35	0.13
sd(7)	0.95	0.31	1.13	0.64	0.07	0.69	0.49	0.03	0.16	0.00								
TGVT-5	44.18	1.54	7.74	12.00	0.41	8.79	22.47	0.47	0.17	0.02	97.80	0.786	0.062	0.036	0.061	0.100	0.42	0.18
sd(7)	0.84	0.31	0.49	0.21	0.03	0.10	0.55	0.02	0.06	0.02								
TGVT-6	42.08	1.62	10.43	13.46	0.43	6.96	23.64	0.49	0.14	0.00	99.27	0.771	0.039	0.037	0.096	0.126	0.34	0.28
sd(8)	0.66	0.06	0.64	1.04	0.10	0.97	0.12	0.03	0.03	0.00								
TGVT-7	44.31	1.56	8.97	11.19	0.40	7.68	21.91	0.57	0.47	0.12	97.17	0.739	0.041	0.044	0.118	0.068	0.41	0.23
sd(7)	0.43	0.01	0.91	0.16	0.12	0.76	0.20	0.04	0.30	0.10								
TGVT-8	44.82	1.73	8.55	12.54	0.46	8.33	23.04	0.56	0.23	0.00	100.27	0.777	0.052	0.042	0.069	0.104	0.40	0.17
sd(7)	0.57	0.31	0.89	0.39	0.04	0.43	0.34	0.08	0.09	0.00								
TGVT-9	43.57	1.78	8.11	12.55	0.51	7.83	22.53	0.54	0.18	0.03	97.65	0.787	0.045	0.042	0.062	0.107	0.38	0.21
sd(7)	0.48	0.34	0.26	0.40	0.11	1.01	0.40	0.05	0.04	0.05								
TGVT-10	46.25	1.39	7.16	9.72	0.40	9.87	22.89	0.50	0.32	0.03	98.54	0.801	0.040	0.037	0.071	0.073	0.50	0.19
sd(9)	0.55	0.18	0.70	0.30	0.04	0.25	0.33	0.04	0.14	0.03								
TGVT-12	46.24	1.24	6.32	9.53	0.36	9.99	23.26	0.38	0.19	0.03	97.54	0.840	0.025	0.029	0.062	0.069	0.51	0.17
sd(6)	0.96	0.28	0.84	0.21	0.04	0.43	0.25	0.08	0.01	0.05								
TGVT-13	47.57	1.04	6.63	11.37	0.28	9.08	23.02	0.50	0.18	0.00	99.67	0.812	0.034	0.037	0.080	0.051	0.44	0.18
sd(4)	1.40	0.08	0.66	3.10	0.08	1.15	0.27	0.09	0.05	0.00								
TGVT-14	46.90	1.19	5.83	10.72	0.49	9.71	22.34	0.47	0.18	0.01	97.85	0.815	0.048	0.036	0.056	0.060	0.48	0.14
sd(8)	0.79	0.09	0.88	0.72	0.06	0.75	0.30	0.06	0.03	0.02								
Trachite (Grotte dei Palizzi)																		

VGPL-1	51.52	0.51	2.83	9.14	0.27	13.61	20.58	0.33	0.10	0.03	98.94	0.779	0.136	0.024	0.040	0.010	0.60	0.26
sd(5)	1.12	0.06	0.83	0.33	0.02	0.67	0.26	0.07	0.04	0.02								
VGPL-2	46.11	0.54	6.31	12.80	0.30	9.19	21.68	0.51	0.12	0.12	97.68	0.787	0.086	0.039	0.066	0.061	0.42	0.36
sd(7)	1.63	0.15	1.12	1.41	0.08	1.25	0.18	0.05	0.03	0.04								
VGPL-3	49.83	0.39	2.86	8.39	0.32	13.77	21.81	0.42	0.12	0.09	97.98	0.844	0.104	0.031	0.003	0.046	0.62	0.21
sd(7)	1.51	0.11	1.08	1.64	0.08	1.37	0.15	0.02	0.03	0.06								
VGPL-4	49.05	0.66	4.52	11.11	0.31	11.76	20.62	0.45	0.14	0.10	98.72	0.760	0.133	0.033	0.048	0.038	0.51	0.30
sd(8)	0.42	0.13	0.58	1.62	0.09	1.32	0.74	0.13	0.03	0.06								
VGPL-5	49.40	0.65	4.89	11.54	0.32	11.42	21.26	0.42	0.15	0.00	100.04	0.768	0.120	0.031	0.055	0.038	0.50	0.33
sd(8)	0.98	0.09	0.71	0.42	0.05	0.38	0.70	0.05	0.16	0.00								
VGPL-6	48.69	0.55	4.47	11.51	0.34	11.44	20.38	0.47	0.18	0.08	98.10	0.759	0.136	0.035	0.047	0.037	0.50	0.24
sd(6)	1.65	0.03	0.69	0.30	0.05	0.17	0.43	0.08	0.06	0.05								
VGPL-7	51.71	0.27	1.96	8.94	0.35	14.81	20.55	0.44	0.19	0.01	99.23	0.798	0.156	0.032	0.000	0.029	0.62	0.22
sd(8)	0.63	0.15	0.57	1.26	0.09	0.44	0.50	0.08	0.12	0.02								
VGPL-8	51.15	0.42	2.59	7.53	0.21	14.35	21.57	0.43	0.13	0.04	98.43	0.830	0.107	0.032	0.014	0.028	0.66	0.20
sd(8)	0.77	0.05	0.54	0.74	0.05	0.69	0.20	0.08	0.03	0.03								
VGPL-9	49.84	0.42	4.25	10.16	0.27	12.64	21.27	0.47	0.14	0.00	99.45	0.784	0.125	0.035	0.039	0.039	0.55	0.29
sd(8)	0.67	0.08	0.45	0.71	0.04	0.35	0.25	0.02	0.08	0.00								
VGPL-10	51.52	0.43	2.76	7.56	0.26	14.61	22.34	0.45	0.10	0.00	100.03	0.846	0.100	0.032	0.005	0.040	0.66	0.23
sd(6)	0.61	0.01	0.39	0.18	0.06	0.22	0.49	0.06	0.05	0.00								

table 5
Click here to download table: Table 5.doc

Table 5. Major element compositions of glasses from phase equilibria experiments performed in this study. Analyses are reported to 100 wt.% on anhydrous basis. sd = standard deviation calculated for the number of analyses in parenthesis.

Run	SiO_2	TiO_2	Al_2O_3	FeO	MnO	MgO	CaO	Na_2O	K_2O	P_2O_5	Total	mg-*number*
Phonolite (Tufo Giallo della Via Tiberina)												
TGVT-1	59.63	0.42	21.23	2.33	0.14	0.20	2.57	4.35	9.11	0.03	100.00	0.08
sd(7)	0.41	0.05	0.29	0.23	0.05	0.03	0.08	0.11	0.19	0.02		
TGVT-2	58.88	0.26	22.47	2.11	0.17	0.14	2.27	4.19	9.50	0.01	100.00	0.06
sd(3)	0.28	0.04	0.75	0.09	0.03	0.03	0.16	0.09	1.04	0.02		
TGVT-3	58.82	0.40	20.61	2.46	0.13	0.18	2.88	4.71	9.77	0.04	100.00	0.07
sd(9)	0.34	0.07	0.26	0.20	0.03	0.05	0.25	0.12	0.18	0.03		
TGVT-4	58.65	0.54	20.16	2.89	0.16	0.21	3.11	5.04	9.18	0.06	100.00	0.07
sd(7)	0.09	0.06	0.10	0.04	0.06	0.03	0.13	0.10	0.12	0.05		
TGVT-5	59.30	0.51	20.94	2.63	0.16	0.35	3.73	3.86	8.45	0.08	100.00	0.12
sd(7)	0.70	0.08	0.43	0.12	0.04	0.05	0.31	0.13	0.19	0.03		
TGVT-6	58.36	0.46	20.89	2.45	0.10	0.36	3.91	4.43	8.99	0.05	100.00	0.13
sd(8)	0.35	0.06	0.18	0.07	0.04	0.03	0.11	0.08	0.09	0.02		
TGVT-7	59.14	0.52	20.33	2.46	0.13	0.39	4.17	4.18	8.61	0.07	100.00	0.14
sd(7)	0.34	0.07	0.33	0.24	0.04	0.05	0.18	0.10	0.17	0.03		
TGVT-8	57.78	0.52	20.54	2.72	0.15	0.30	3.30	4.97	9.65	0.07	100.00	0.10
sd(7)	0.19	0.06	0.23	0.10	0.06	0.03	0.23	0.08	0.14	0.04		
TGVT-9	58.81	0.53	20.45	2.42	0.12	0.32	3.37	4.41	9.51	0.05	100.00	0.12
sd(7)	0.33	0.09	0.11	0.22	0.05	0.04	0.26	0.11	0.23	0.03		
TGVT-10	58.66	0.53	20.17	2.80	0.15	0.54	4.38	4.16	8.53	0.07	100.00	0.16
sd(9)	0.21	0.08	0.23	0.10	0.04	0.07	0.12	0.09	0.19	0.03		
TGVT-11	57.60	0.49	20.77	2.55	0.17	0.61	5.07	4.14	8.52	0.09	100.00	0.19
sd(6)	0.46	0.04	0.17	0.37	0.05	0.04	0.14	0.17	0.16	0.02		
TGVT-12	58.07	0.52	20.47	2.85	0.15	0.51	4.45	4.19	8.71	0.08	100.00	0.15
sd(8)	0.40	0.09	0.23	0.14	0.04	0.06	0.24	0.06	0.14	0.01		
TGVT-13	57.91	0.48	19.86	3.25	0.13	0.46	4.77	4.47	8.55	0.11	100.00	0.13
sd(7)	0.17	0.05	0.13	0.10	0.03	0.05	0.17	0.07	0.09	0.03		
TGVT-14	58.62	0.53	20.46	3.17	0.16	0.41	3.84	4.07	8.66	0.08	100.00	0.11
sd(8)	0.43	0.06	0.31	0.16	0.04	0.04	0.40	0.09	0.17	0.02		

Trachite (Grotte dei Palizzi)												
VGPL-1	60.36	0.50	16.89	4.91	0.13	1.92	4.36	4.19	6.44	0.30	100.00	0.28
sd(5)	0.21	0.03	0.21	0.08	0.05	0.09	0.13	0.11	0.07	0.01		
VGPL-2	66.98	0.39	18.79	2.42	0.09	0.63	2.19	2.38	6.00	0.14	100.00	0.21
sd(7)	0.35	0.04	0.43	0.16	0.03	0.13	0.24	0.10	0.12	0.04		
VGPL-3	62.40	0.50	17.76	3.28	0.08	1.12	3.13	4.76	6.76	0.22	100.00	0.26
sd(7)	0.52	0.07	0.38	0.44	0.05	0.10	0.24	0.13	0.12	0.07		
VGPL-4	62.41	0.48	18.43	2.49	0.07	0.78	2.46	5.20	7.35	0.32	100.00	0.24
sd(8)	0.60	0.11	0.36	0.16	0.06	0.05	0.13	0.24	0.10	0.12		
VGPL-5	63.52	0.47	18.19	2.60	0.07	0.85	2.65	4.76	6.59	0.31	100.00	0.25
sd(8)	0.28	0.07	0.17	0.34	0.05	0.06	0.15	0.11	0.09	0.09		
VGPL-6	64.59	0.35	18.20	2.99	0.09	0.71	2.11	4.04	6.72	0.20	100.00	0.19
sd(6)	0.66	0.08	0.36	0.17	0.05	0.12	0.23	0.11	0.20	0.05		
VGPL-7	62.03	0.46	17.94	3.16	0.09	1.18	3.15	4.97	6.78	0.24	100.00	0.27
sd(8)	0.40	0.09	0.35	0.38	0.04	0.15	0.29	0.05	0.18	0.08		
VGPL-8	61.46	0.48	17.44	3.65	0.12	1.38	3.76	4.81	6.52	0.38	100.00	0.27
sd(8)	0.66	0.05	0.17	0.29	0.04	0.11	0.29	0.17	0.11	0.04		
VGPL-9	61.83	0.46	17.67	3.81	0.08	1.37	3.62	4.62	6.18	0.35	100.00	0.26
sd(8)	0.20	0.05	0.12	0.14	0.04	0.07	0.22	0.08	0.10	0.02		
VGPL-10	60.05	0.57	16.80	4.98	0.11	2.17	4.50	4.12	6.38	0.32	100.00	0.30
sd(6)	0.44	0.07	0.32	0.23	0.06	0.08	0.17	0.16	0.10	0.07		

Cpx-Liq alkali thermobarometer

Click here to download Electronic supplementary material: Cpx-Liq alkali thermobarometer.xlsx

Tables EA

Click here to download Electronic supplementary material: Tables EA.pdf